

AIM2 forms a complex with pyrin and ZBP1 to drive PANoptosis and host defence

<https://doi.org/10.1038/s41586-021-03875-8>

Received: 17 March 2021

Accepted: 4 August 2021

Published online: 1 September 2021

 Check for updates

SangJoon Lee¹, Rajendra Karki¹, Yaqiu Wang¹, Lam Nhat Nguyen¹, Ravi C. Kalathur² & Thirumala-Devi Kanneganti¹✉

Inflammasomes are important sentinels of innate immune defence, sensing pathogens and inducing cell death in infected cells¹. There are several inflammasome sensors that each detect and respond to a specific pathogen- or damage-associated molecular pattern (PAMP or DAMP, respectively)¹. During infection, live pathogens can induce the release of multiple PAMPs and DAMPs, which can simultaneously engage multiple inflammasome sensors^{2–5}. Here we found that AIM2 regulates the innate immune sensors pyrin and ZBP1 to drive inflammatory signalling and a form of inflammatory cell death known as PANoptosis, and provide host protection during infections with herpes simplex virus 1 and *Francisella novicida*. We also observed that AIM2, pyrin and ZBP1 were members of a large multi-protein complex along with ASC, caspase-1, caspase-8, RIPK3, RIPK1 and FADD, that drove inflammatory cell death (PANoptosis). Collectively, our findings define a previously unknown regulatory and molecular interaction between AIM2, pyrin and ZBP1 that drives assembly of an AIM2-mediated multi-protein complex that we term the AIM2 PANoptosome and comprising multiple inflammasome sensors and cell death regulators. These results advance the understanding of the functions of these molecules in innate immunity and inflammatory cell death, suggesting new therapeutic targets for AIM2-, ZBP1- and pyrin-mediated diseases.

Inflammasomes are critical components of the innate immune response¹. Following exposure to PAMPs and DAMPs, inflammasome sensors form a multi-protein complex that activates caspase-1, leading to cleavage of its downstream substrates, inflammatory signalling and inflammatory cell death. Individual inflammasome sensors detect and respond to specific PAMPs and DAMPs, but emerging evidence suggests that multiple inflammasome sensors can be activated in response to disease, particularly live pathogen infection, owing to the presence of multiple PAMPs and DAMPs^{2–5}.

The AIM2 inflammasome is known to sense double-stranded DNA (dsDNA) and has essential roles in development, infectious diseases, inflammatory diseases and cancer^{6–11}. However, several critical functions of AIM2 beyond its canonically described role in inflammasome formation and pyroptosis have been observed that cannot be explained by our current understanding of the AIM2 inflammasome². Herpes simplex virus 1 (HSV1), a dsDNA virus that causes lifelong incurable, recurrent pathologies, and *Francisella*, a Gram-negative bacterium that can cause rapid lethality upon infection, are two diverse pathogens that are known to activate the AIM2 inflammasome and cell death^{6,10–13}. To investigate whether cells exposed to numerous PAMPs and DAMPs during these viral and bacterial infections can simultaneously engage multiple inflammasome sensors, we infected wild-type bone marrow-derived macrophages (BMDMs) and BMDMs singly deficient in several major inflammasome sensors with HSV1 or *F. novicida*. Infection with HSV1 or *F. novicida* induced AIM2-dependent and

NLRP3- and NLRC4-independent cleavage of caspase-1, release of the inflammasome-dependent cytokines interleukin (IL)-1 β and IL-18, and cell death (Fig. 1a–o, Extended Data Fig. 1a–i). However, inflammasome activation and cell death were also partially reduced in *Mefv*^{-/-} BMDMs during HSV1 and *F. novicida* infections (Fig. 1p–t, Extended Data Fig. 1j–l), suggesting that these infections activate pyrin to drive AIM2-mediated inflammatory signalling and cell death.

Because we observed residual AIM2-mediated caspase cleavage in *Mefv*^{-/-} BMDMs after HSV1 and *F. novicida* infections (Fig. 1p, Extended Data Fig. 1j), we screened several innate immune sensors to determine their involvement. Loss of the sensor ZBP1, which regulates inflammatory cell death in infectious and sterile conditions^{14–16}, resulted in reduced caspase-1 cleavage, release of IL-1 β and IL-18 and cell death compared with wild-type BMDMs after HSV1 and *F. novicida* infections (Fig. 1u–y, Extended Data Fig. 1m–o), whereas loss of other sensors or adaptors had no effect (Extended Data Fig. 2), suggesting that ZBP1 is also involved in HSV1- and *F. novicida*-induced inflammatory signalling and cell death.

To determine whether pyrin and ZBP1 act cooperatively or redundantly to decrease caspase-1 activation and cell death, we next used colchicine to inhibit pyrin activation^{17,18} in *Zbp1*^{-/-} BMDMs. We found that colchicine treatment in *Zbp1*^{-/-} BMDMs further reduced cell death, cleavage of caspase-1 and release of IL-1 β and IL-18 during HSV1 and *F. novicida* infections, mirroring the levels observed in *Aim2*^{-/-} BMDMs (Fig. 2a, b, Extended Data Fig. 3), suggesting that ZBP1 cooperates with

¹Department of Immunology, St Jude Children's Research Hospital, Memphis, TN, USA. ²Department of Structural Biology, St Jude Children's Research Hospital, Memphis, TN, USA.

✉e-mail: Thirumala-Devi.Kanneganti@StJude.org

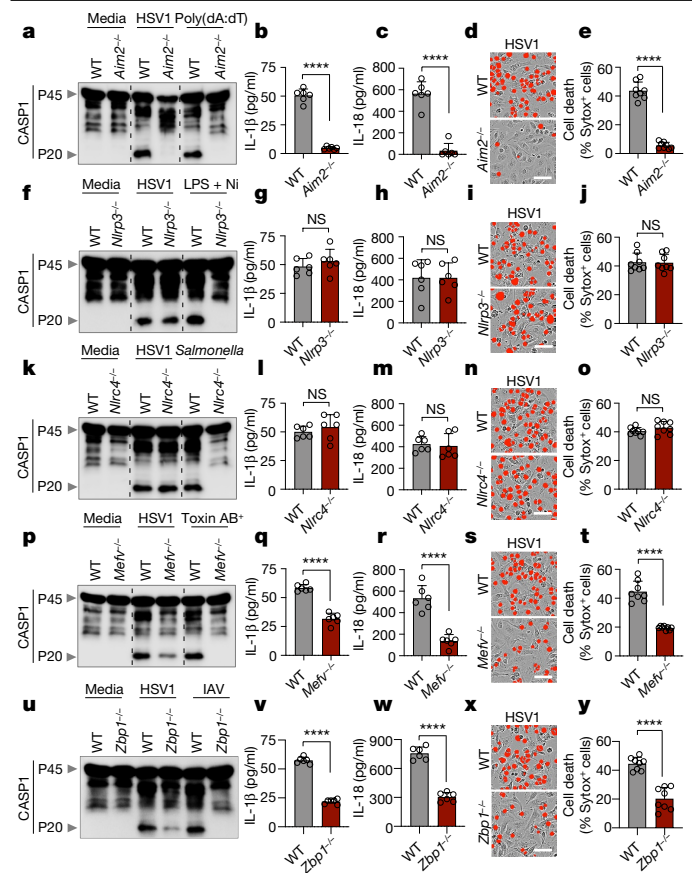


Fig. 1 | HSV1 induces AIM2-, pyrin- and ZBP1-mediated caspase-1 activation, cytokine release and cell death. **a**, Immunoblot analysis of pro-caspase-1 (P45) and cleaved caspase-1 (CASP1) (P20) in HSV1-infected or poly(dA:dT)-transfected wild-type (WT) or *Aim2*^{-/-} BMDMs. **b**, **c**, IL-1β (**b**) and IL-18 (**c**) release following HSV1 infection. **d**, Cell death in BMDMs after HSV1 infection for 16 h, measured by SYTOX Green uptake assay. Red indicates dead cells. **e**, Quantification of the cell death in **d**. **f**–**j**, Immunoblot analysis of CASP1 (**f**), release of IL-1β (**g**) and IL-18 (**h**), cell death images at 16 h after infection (**i**) and quantification of cell death (**j**) from WT or *Nlrp3*^{-/-} BMDMs after HSV1 infection or lipopolysaccharide (LPS) plus nigericin (Ni) treatment. **k**–**o**, Immunoblot analysis of CASP1 (**k**), release of IL-1β (**l**) and IL-18 (**m**), cell death images at 16 h after infection (**n**) and quantification of cell death (**o**) from WT or *Nlr4*^{-/-} BMDMs after HSV1 or *Salmonella* Typhimurium infection. **p**–**t**, Immunoblot analysis of CASP1 (**p**), release of IL-1β (**q**) and IL-18 (**r**), cell death images at 16 h after infection (**s**) and quantification of cell death (**t**) from WT or *Mefv*^{-/-} BMDMs after HSV1 infection or *C. difficile* toxin AB⁺ supernatant treatment. **u**–**y**, Immunoblot analysis of CASP1 (**u**), release of IL-1β (**v**) and IL-18 (**w**), cell death images at 16 h after infection (**x**), and quantification of cell death (**y**) from WT or *Zbp1*^{-/-} BMDMs after HSV1 or influenza A virus (IAV) infection. **a**, **f**, **k**, **p**, **u**. Data are representative of at least three independent experiments. **b**, **c**, **g**, **h**, **l**, **m**, **q**, **r**, **v**, **w**. Data are mean ± s.e.m. NS, not significant; *****P* < 0.0001 (two-tailed *t*-test; *n* = 6 from 3 biologically independent samples). **d**, **i**, **n**, **s**, **x**. Images are representative of at least three independent experiments. Scale bars, 50 μm. **e**, **j**, **o**, **t**, **y**. Data are mean ± s.e.m. NS, not significant; *****P* < 0.0001 (two-tailed *t*-test; *n* = 8 from 4 biologically independent samples). Exact *P* values are presented in Supplementary Table 1. For gel source data, see Supplementary Figure 1.

pyrin to drive the AIM2-dependent responses. We also generated *Mefv*^{-/-} *Zbp1*^{-/-} mice and found that cell death, cleavage of caspase-1 and release of IL-1β and IL-18 during HSV1 and *F. novicida* infections were further reduced in *Mefv*^{-/-} *Zbp1*^{-/-} BMDMs compared with *Mefv*^{-/-} or *Zbp1*^{-/-} BMDMs, mirroring the levels observed in *Aim2*^{-/-} BMDMs (Fig. 2c–j, Extended Data Fig. 4a, b). These results suggest that pyrin and ZBP1 cooperate to induce AIM2-mediated inflammatory signalling and cell death during both viral infection with HSV1 and bacterial infection with *F. novicida*. Similarly, we also observed activation of cell death and

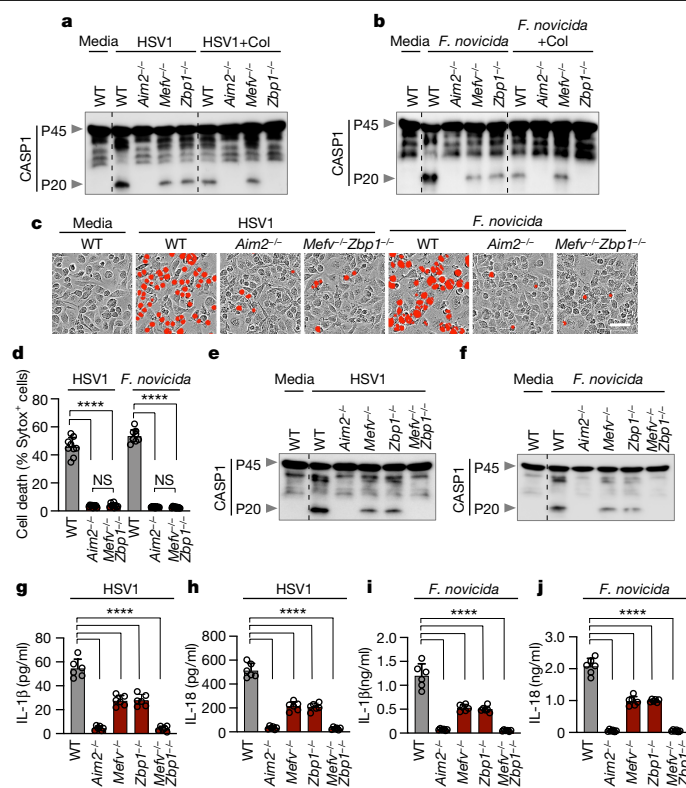


Fig. 2 | ZBP1 cooperates with pyrin to drive AIM2-mediated caspase-1 activation, cytokine release and cell death. **a**, **b**, Immunoblot analysis of caspase-1 in BMDMs infected with HSV1 or *F. novicida* with or without colchicine (Col). Data are representative of at least three independent experiments. **c**, Cell death in wild-type, *Aim2*^{-/-} or *Mefv*^{-/-} *Zbp1*^{-/-} BMDMs at 16 h after infection with HSV1 or *F. novicida*. Red indicates dead cells. Data are representative of at least three independent experiments. Scale bar, 50 μm. **d**, Quantification of the cell death from **c**. Data are mean ± s.e.m. (one-way ANOVA with Dunnett’s multiple comparisons test; *n* = 9 from 3 biologically independent samples). **e**, **f**, Immunoblot analysis of CASP1 in BMDMs infected with HSV1 (**e**) or *F. novicida* (**f**). Data are representative of at least three independent experiments. **g**–**j**, Release of IL-1β (**g**, **i**) or IL-18 (**h**, **j**) following HSV1 (**g**, **h**) or *F. novicida* (**i**, **j**) infection. Data are mean ± s.e.m. (one-way ANOVA with Dunnett’s multiple comparisons test; *n* = 6 from 3 biologically independent samples). Exact *P* values are presented in Supplementary Table 1. For gel source data, see Supplementary Figure 1.

caspase-1 in human THP-1 macrophages during HSV1 infection, and this activation was inhibited by short interfering RNA (siRNA) knockdown of AIM2 or combined knockdown of ZBP1 and MEFV (Extended Data Fig. 4c–e), suggesting that the AIM2- and pyrin and ZBP1-mediated cell death also occurs in human cells, the natural host of HSV1. Furthermore, the extent of cell death and caspase-1 cleavage was similar between wild-type and *Mefv*^{-/-}, *Zbp1*^{-/-} or *Mefv*^{-/-} *Zbp1*^{-/-} BMDMs treated with the synthetic AIM2 inflammasome ligand poly(dA:dT) (Extended Data Fig. 4f–h), suggesting that infection is a unique trigger causing pyrin and ZBP1 to cooperate to facilitate AIM2-mediated caspase-1 activation, cytokine release and cell death.

To understand how pyrin is activated during HSV1 and *F. novicida* infections, we first evaluated RhoA-GTP activity, which is known to be inhibited to activate pyrin in response to bacterial toxins such as the *Clostridium difficile* toxin TcdB^{17–21}. We found that TcdB-mediated inhibition of RhoA-GTP activity occurred in an AIM2- and ZBP1-independent manner (Extended Data Fig. 5a), whereas HSV1-mediated inhibition was dependent on AIM2 but independent of ZBP1 (Extended Data Fig. 5a). We next examined RhoA-GTP levels in *Aim2*^{-/-}, *Asc*^{-/-} and *Casp1*^{-/-} BMDMs during HSV1 and *F. novicida* infections. Whereas RhoA-GTP was absent

in wild-type BMDMs upon infection, it was present in *Aim2*^{-/-}, *Asc*^{-/-} and *Casp1*^{-/-} BMDMs (Extended Data Fig. 5b, c). By contrast, treatment with the synthetic AIM2 inflammasome ligand poly(dA:dT) did not inhibit RhoA-GTP activity in any of the genotypes tested (Extended Data Fig. 5d, e), suggesting that infection has a distinct ability to integrate the AIM2-mediated signalling and RhoA-signalling cascades to influence pyrin activation.

We then investigated how ZBP1 was activated during HSV1 and *F. novicida* infections. In the context of influenza A virus infection, ZBP1 Zα domains sense nucleic acids to drive RIPK3-, caspase-8- and NLRP3-mediated inflammatory cell death^{14,15,22}. Similarly, we found that HSV1- and *F. novicida*-induced cell death was reduced in *Zbp1*^{ΔZα2/ΔZα2} BMDMs compared with wild-type BMDMs and was similar to that of *Zbp1*^{-/-} BMDMs (Extended Data Fig. 5f–i).

Our data show that HSV1 and *F. novicida* can activate multiple inflammasome sensors. Many pathogens can also induce multiple programmed cell death pathways, including pyroptosis, apoptosis and necroptosis^{14,23}. Recent studies have found extensive crosstalk between programmed cell death pathways^{14,24–27}, establishing the concept of PANoptosis^{14,28–31}. Although inflammasome activation is primarily associated with gasdermin D (GSDMD)-mediated pyroptosis, there is emerging evidence of a contribution of inflammasome components in driving PANoptosis^{14,15,26,27,29,30,32}. Therefore, we biochemically characterized the cell death induced by HSV1 and *F. novicida* infections. In wild-type cells, HSV1 and *F. novicida* activated key molecules involved in pyroptotic, apoptotic and necroptotic pathways (Fig. 3). However, we observed reduced activation of the pyroptotic molecules caspase-1, GSDMD and GSDME (Fig. 3a), the apoptotic molecules caspase-8, -3 and -7 (Fig. 3b) and the necroptotic molecules RIPK3 and MLKL (Fig. 3c) in *Mefv*^{-/-} and *Zbp1*^{-/-} BMDMs compared with wild-type BMDMs following HSV1 or *F. novicida* infection, and a complete loss of activation in *Aim2*^{-/-} and *Mefv*^{-/-}*Zbp1*^{-/-} BMDMs. Collectively, these data suggest that HSV1 and *F. novicida* infections induce inflammatory cell death, PANoptosis, in a manner dependent on AIM2 and the coordinated activation of pyrin and ZBP1.

We next sought to understand the regulatory relationship between AIM2, pyrin and ZBP1 during infection with HSV1 or *F. novicida*. Loss of AIM2 completely abrogated the inflammatory cell death, whereas loss of pyrin or ZBP1 resulted in a partial reduction, suggesting that AIM2 functions upstream of pyrin and ZBP1. Protein expression of pyrin and ZBP1 was reduced in *Aim2*^{-/-} BMDMs after HSV1 or *F. novicida* infection (Fig. 4a, b). Additionally, their expression was also reduced in *Asc*^{-/-}, *Casp1*^{-/-} and enzymatically inactive *Casp1*^{C284A/C284A} BMDMs as well as in wild-type BMDMs treated with the caspase-1 inhibitor VX-765 (Fig. 4c, d), but not in *Gsdmd*^{-/-}, *Casp8*^{DA/DA}, *Casp7*^{-/-}, *Casp3*^{-/-} or *Casp6*^{-/-} BMDMs after HSV1 and *F. novicida* infections (Extended Data Fig. 6a–c). Furthermore, expression of pyrin and ZBP1 was not affected during influenza A virus infection in *Aim2*^{-/-}, *Asc*^{-/-}, *Casp1*^{-/-} and *Nlrp3*^{-/-} BMDMs (Extended Data Fig. 6d). Therefore, AIM2-mediated signalling functions as an upstream regulator for the expression of pyrin and ZBP1 in response to HSV1 and *F. novicida* infections.

To investigate the molecular mechanism underlying how AIM2, ASC and caspase-1 activity-dependent signals promote the expression of pyrin and ZBP1 in infected cells, we assessed transcription and observed that HSV1- or *F. novicida*-infected *Aim2*^{-/-}, *Asc*^{-/-} and *Casp1*^{-/-} BMDMs had reduced transcription of *Zbp1* and *Mefv* compared with the levels in wild-type cells (Extended Data Fig. 7a–d). It was previously shown that expression of pyrin and ZBP1 can be induced by interferon (IFN) signalling^{14,33}. Therefore, we investigated whether AIM2 could induce IFN production to drive the expression of pyrin and ZBP1. We found that wild-type BMDMs produced IFN-β in response to HSV1 (multiplicity of infection (MOI) 10, 6 h after infection) or *F. novicida* infection (MOI 1, 3 h after infection), whereas *Aim2*^{-/-}, *Asc*^{-/-} and *Casp1*^{-/-} BMDMs did not (Extended Data Fig. 7e, f). Additionally, the expression of pyrin and ZBP1 was restored upon complementation of IFN-β in the AIM2-, ASC- and

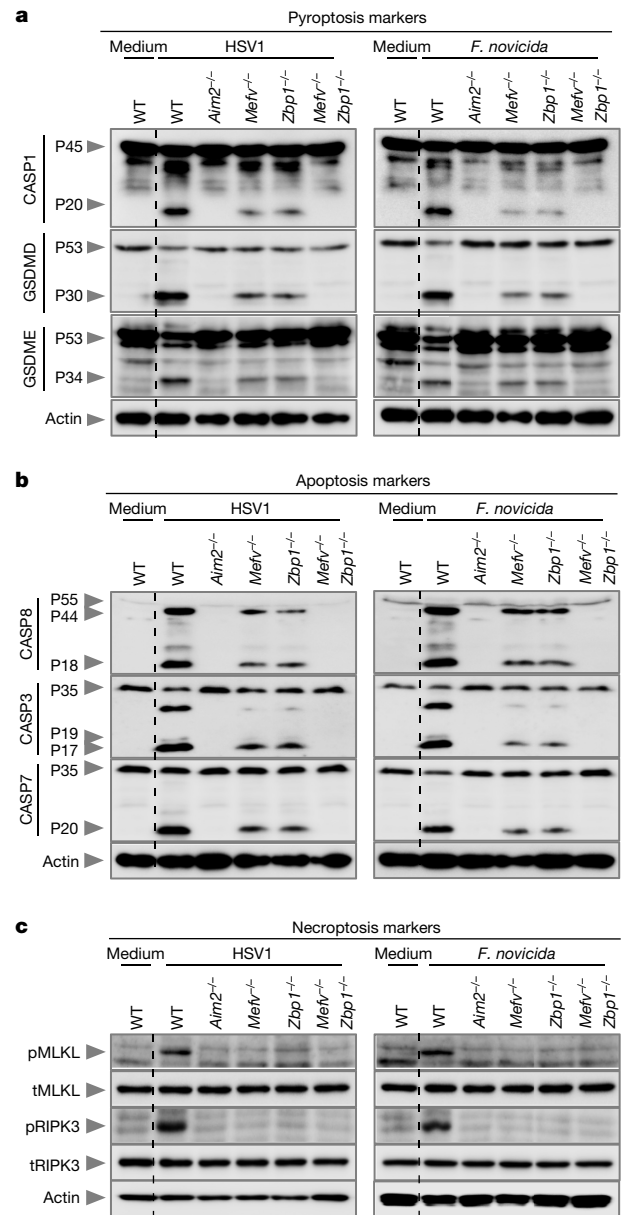


Fig. 3 | AIM2, pyrin and ZBP1 promote inflammatory cell death in response to HSV1 and *F. novicida* infections. a–c, Immunoblot analysis of pro- (P45) and activated (P20) caspase-1 (CASP1), pro- (P53) and activated (P30) GSDMD, pro- (P53) and activated (P34) GSDME (a); pro- (P55) and cleaved (P18) caspase-8 (CASP8), pro- (P35) and cleaved (P17/P19) caspase-3 (CASP3), pro- (P35) and cleaved (P20) caspase-7 (CASP7) (b); phosphorylated MLKL (pMLKL), total MLKL (tMLKL), phosphorylated RIPK3 (pRIPK3) and total RIPK3 (tRIPK3) (c) in wild-type, *Aim2*^{-/-}, *Mefv*^{-/-}, *Zbp1*^{-/-} or *Mefv*^{-/-}*Zbp1*^{-/-} BMDMs after HSV1 or *F. novicida* infection. Data are representative of at least three independent experiments. For gel source data, see Supplementary Figure 1.

caspase-1-deficient cells (Extended Data Fig. 7g, h). The differences in IFN production observed here are in contrast to previous studies with *F. novicida*, in which these knockouts have not been reported to have a marked loss of type I IFN production. These differences might be due to differing timepoints and MOIs: previous studies showed that *Asc*^{-/-} BMDMs have slightly reduced IFN-β release 5 h after infection³⁴ (MOI 100) and similar *ifnb* mRNA levels 9 h after infection³⁵ (MOI 100); *Aim2*^{-/-} BMDMs have significantly increased IFN-β release 6 h after infection¹¹ (MOI 250); and *Asc*^{-/-} and *Casp1*^{-/-} BMDMs have significantly increased IFN-β release 6 h after infection³⁶ (MOI 50). These

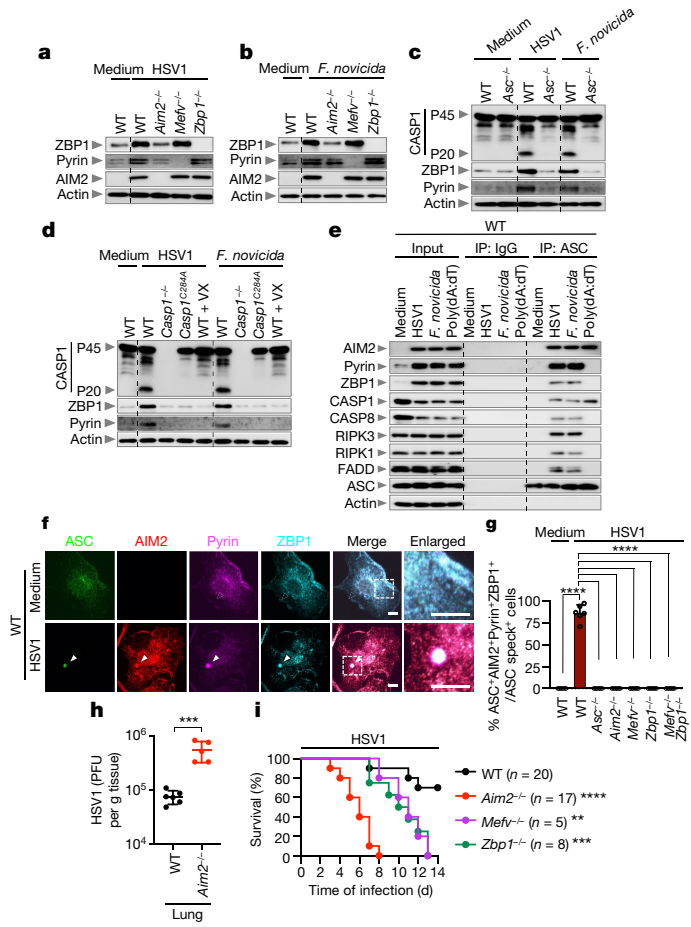


Fig. 4 | AIM2-mediated signalling acts as an upstream regulator of pyrin and ZBP1, which are required to form the AIM2 PANoptosome.
a, b, Immunoblot analysis of ZBP1, pyrin and AIM2 in wild-type, *Aim2*^{-/-}, *Mef1*^{-/-} and *Zbp1*^{-/-} BMDMs infected with HSV1 (**a**) or *F. novicida* (**b**). **c**, Immunoblot analysis of caspase-1 (CASP1) activation and pyrin and ZBP1 expression in wild-type or *Asc*^{-/-} BMDMs after HSV1 or *F. novicida* infection. **d**, Immunoblot analysis of CASP1 activation and pyrin and ZBP1 expression in wild-type, *Casp1*^{-/-} and *Casp1*^{C284A/C284A} (*Casp1*^{C284A}) BMDMs and wild-type BMDMs treated with the CASP1 inhibitor VX-765 (20 μM; VX) after HSV1 or *F. novicida* infection. **e**, Immunoprecipitation (IP) in wild-type BMDMs with IgG control antibodies or anti-ASC antibodies after HSV1 or *F. novicida* infection or poly(dA:dT) transfection. **a–e**, Data are representative of at least three independent experiments. **f**, Immunofluorescence images of wild-type BMDMs at 12 h after HSV1 infection. Scale bars, 5 μm. Arrowheads indicate the ASC speck. Images are representative of three independent experiments. **g**, Quantification of the percentage of cells with ASC-AIM2-pyrin-ZBP1+ specks among the ASC speck+ cells. Data are mean ± s.e.m. (one-way ANOVA with Dunnett’s multiple comparisons test; *n* = 6 from 3 biologically independent samples). **h**, Pulmonary viral titre at day 3 after infection with HSV1 (WT, *n* = 6; *Aim2*^{-/-}, *n* = 5). Each symbol represents one mouse. Data are pooled from two independent experiments. Data are mean ± s.e.m. ****P* < 0.001 (two-tailed t-test). **i**, Survival of wild-type, *Aim2*^{-/-}, *Mef1*^{-/-} and *Zbp1*^{-/-} mice infected intranasally with 5 × 10⁷ plaque-forming units (PFU) of HSV1. Survival data are pooled from three independent experiments. *P* values for survival of each genotype versus wild type are shown in the key. ***P* < 0.01; ****P* < 0.001; *****P* < 0.0001 (log-rank (Mantel–Cox) test). Exact *P* values are presented in Supplementary Table 1. For gel source data, see Supplementary Figure 1.

differences suggest that type I IFN release in response to *F. novicida* may be timepoint- and/or MOI-dependent.

Next, we sought to understand the molecular relationship between AIM2, pyrin and ZBP1 in inducing inflammatory cell death and PANoptosis during HSV1 and *F. novicida* infections. We hypothesized that these

molecules would all be part of the molecular scaffold that enables contemporaneous engagement of key proteins from pyroptosis, apoptosis and necroptosis^{28,29,31,32}. We observed interactions of ASC with AIM2, pyrin, ZBP1, caspase-1, caspase-8, RIPK3, RIPK1 and FADD by immunoprecipitation following HSV1 and *F. novicida* infections (Fig. 4e), and these interactions were not observed in *Aim2*^{-/-}, *Mef1*^{-/-}, *Zbp1*^{-/-}, *Ripk3*^{-/-}, *Casp8*^{-/-} or *Ripk1*^{-/-} BMDMs (Extended Data Fig. 8). By contrast, treatment with poly(dA:dT) allowed interactions between endogenous ASC, AIM2 and caspase-1, but not pyrin, ZBP1, caspase-8, RIPK3, RIPK1 or FADD (Fig. 4e), suggesting that infection has a distinct ability to form this AIM2 multi-protein cell death-inducing complex. We have termed this complex the AIM2 PANoptosome. We also observed that ASC specks colocalized with AIM2, pyrin and ZBP1 collectively in the same cell at 12 h after infection with HSV1 or *F. novicida* (Fig. 4f, g, Extended Data Fig. 9a, b). Similarly, ASC specks also colocalized with caspase-8 and RIPK3 in the same cell (Extended Data Fig. 9c–f). Furthermore, the formation of this complex was required for cell death, as its disruption through the deletion of key components inhibited cell death in response to HSV1 and *F. novicida* infections (Fig. 2c, d, Extended Data Fig. 9g, h).

We then extended our findings to in vivo models of HSV1 and *F. novicida* infection. Lung lysates from infected wild-type mice showed activation of key pyroptotic, apoptotic and necroptotic molecules and increased expression of pyrin and ZBP1, but this activation and increased expression was not found in *Aim2*^{-/-} mice (Extended Data Fig. 10a, b). The number of plaque- and colony-forming units for HSV1 and *F. novicida*, respectively, was increased in *Aim2*^{-/-}, *Mef1*^{-/-}, *Zbp1*^{-/-} and *Mef1*^{-/-} *Zbp1*^{-/-} BMDMs and in the tissue of *Aim2*^{-/-} mice (Fig. 4h, Extended Data Fig. 10c–e). Additionally, all mice lacking AIM2 succumbed to HSV1 infection within 8 days and mice lacking pyrin or ZBP1 succumbed within 13 days, whereas around 70% of the wild-type mice survived (Fig. 4i). Similarly, all mice lacking AIM2 succumbed to *F. novicida* infection within 4 days and mice lacking pyrin or ZBP1 succumbed within 9 or 11 days, respectively, whereas around 80% of the wild-type mice survived (Extended Data Fig. 10f). These results highlight an important role for the AIM2-regulated expression of pyrin and ZBP1, inflammatory cell death and PANoptosis in host defence against HSV1 and *F. novicida* infections.

In summary, AIM2, pyrin and ZBP1 form a multi-protein complex termed the AIM2 PANoptosome via interactions with ASC to induce PANoptosis during HSV1 and *F. novicida* infections. Loss of AIM2 reduces the expression of pyrin and ZBP1 during these infections, indicating that AIM2-mediated signalling functions as an upstream regulator of pyrin and ZBP1 to control assembly and activation of the AIM2 PANoptosome. The ability of HSV1 and *F. novicida* to activate AIM2 while also engaging the ZBP1 Zα domain and inhibiting Rho-GTP activity gives these pathogens the unique ability to form this AIM2-, pyrin- and ZBP1-containing PANoptosome complex. Other pathogens that can engage multiple sensors may also form similar complexes with shared central components.

Furthermore, we observed roles for ZBP1 in innate immunity. ZBP1 is known to sense influenza viral Z-RNA to promote binding of RIPK3, caspase-6 and the NLRP3 inflammasome to form the ZBP1 PANoptosome complex and drive PANoptosis^{14,15,22,31}. The multi-protein complex identified here is mediated by AIM2 but may be similar to this ZBP1 PANoptosome, as it shares the same cell death effectors, including caspase-8 and RIPK3, and also leads to the induction of PANoptosis, characterized by activation of pyroptotic, apoptotic and necroptotic molecules. Additionally, we discovered that ZBP1 also interacts and localizes with ASC and acts as an inflammasome sensor to induce caspase-1 cleavage and inflammatory cell death in response to HSV1 and *F. novicida* infections. Furthermore, AIM2 regulated the expression of pyrin and ZBP1 during HSV1 and *F. novicida* infections, but not during influenza A virus infection.

Overall, our findings identify a critical interaction between AIM2, pyrin and ZBP1 that drives innate immune responses during pathogen

infection. This regulatory mechanism defines the molecular basis of how infection with live pathogens that liberate numerous PAMPs or DAMPs can trigger the coordinated activation of innate immune and cell death signalling components to form a multi-protein complex and cause inflammatory cell death and cytokine release to shape the immune response and host defence.

Online content

Any methods, additional references, Nature Research reporting summaries, source data, extended data, supplementary information, acknowledgements, peer review information; details of author contributions and competing interests; and statements of data and code availability are available at <https://doi.org/10.1038/s41586-021-03875-8>.

1. Man, S. M., Karki, R. & Kanneganti, T. D. Molecular mechanisms and functions of pyroptosis, inflammatory caspases and inflammasomes in infectious diseases. *Immunol. Rev.* **277**, 61–75 (2017).
2. Karki, R. et al. Concerted activation of the AIM2 and NLRP3 inflammasomes orchestrates host protection against *Aspergillus* infection. *Cell Host Microbe* **17**, 357–368 (2015).
3. Broz, P. et al. Redundant roles for inflammasome receptors NLRP3 and NLRC4 in host defense against *Salmonella*. *J. Exp. Med.* **207**, 1745–1755 (2010).
4. Man, S. M. et al. Inflammasome activation causes dual recruitment of NLRC4 and NLRP3 to the same macromolecular complex. *Proc. Natl Acad. Sci. USA* **111**, 7403–7408 (2014).
5. Kalantari, P. et al. Dual engagement of the NLRP3 and AIM2 inflammasomes by plasmodium-derived hemozoin and DNA during malaria. *Cell Rep.* **6**, 196–210 (2014).
6. Man, S. M. et al. The transcription factor IRF1 and guanylate-binding proteins target activation of the AIM2 inflammasome by *Francisella* infection. *Nat. Immunol.* **16**, 467–475 (2015).
7. Sharma, B. R., Karki, R. & Kanneganti, T. D. Role of AIM2 inflammasome in inflammatory diseases, cancer and infection. *Eur. J. Immunol.* **49**, 1998–2011 (2019).
8. Lammert, C. R. et al. AIM2 inflammasome surveillance of DNA damage shapes neurodevelopment. *Nature* **580**, 647–652 (2020).
9. Hornung, V. et al. AIM2 recognizes cytosolic dsDNA and forms a caspase-1-activating inflammasome with ASC. *Nature* **458**, 514–518 (2009).
10. Rathinam, V. A. et al. The AIM2 inflammasome is essential for host defense against cytosolic bacteria and DNA viruses. *Nat. Immunol.* **11**, 395–402 (2010).
11. Fernandes-Alnemri, T. et al. The AIM2 inflammasome is critical for innate immunity to *Francisella tularensis*. *Nat. Immunol.* **11**, 385–393 (2010).
12. Zhu, Q., Man, S. M., Karki, R., Malireddi, R. K. S. & Kanneganti, T. D. Detrimental type I interferon signaling dominates protective AIM2 inflammasome responses during *Francisella novicida* infection. *Cell Rep.* **22**, 3168–3174 (2018).
13. Maruzuru, Y. et al. Herpes simplex virus 1 VP22 inhibits AIM2-dependent inflammasome activation to enable efficient viral replication. *Cell Host Microbe* **23**, 254–265.e257 (2018).
14. Kuriakose, T. et al. ZBP1/DAI is an innate sensor of influenza virus triggering the NLRP3 inflammasome and programmed cell death pathways. *Sci. Immunol.* **1**, aag2045 (2016).
15. Kesavardhana, S. et al. The Za2 domain of ZBP1 is a molecular switch regulating influenza-induced PANoptosis and perinatal lethality during development. *J. Biol. Chem.* **295**, 8325–8330 (2020).
16. Newton, K. et al. RIPK1 inhibits ZBP1-driven necroptosis during development. *Nature* **540**, 129–133 (2016).
17. Park, Y. H., Wood, G., Kastner, D. L. & Chae, J. J. Pyrin inflammasome activation and Rho signaling in the autoinflammatory diseases FMF and HIDS. *Nat. Immunol.* **17**, 914–921 (2016).
18. Gao, W., Yang, J., Liu, W., Wang, Y. & Shao, F. Site-specific phosphorylation and microtubule dynamics control Pyrin inflammasome activation. *Proc. Natl Acad. Sci. USA* **113**, E4857–E4866 (2016).
19. Xu, H. et al. Innate immune sensing of bacterial modifications of Rho GTPases by the Pyrin inflammasome. *Nature* **513**, 237–241 (2014).
20. Masters, S. L. et al. Familial autoinflammation with neutrophilic dermatosis reveals a regulatory mechanism of pyrin activation. *Sci. Transl. Med.* **8**, 332ra345 (2016).
21. Van Gorp, H. et al. Familial Mediterranean fever mutations lift the obligatory requirement for microtubules in Pyrin inflammasome activation. *Proc. Natl Acad. Sci. USA* **113**, 14384–14389 (2016).
22. Kesavardhana, S. et al. ZBP1/DAI ubiquitination and sensing of influenza vRNPs activate programmed cell death. *J. Exp. Med.* **214**, 2217–2229 (2017).
23. Place, D. E., Lee, S. & Kanneganti, T. D. PANoptosis in microbial infection. *Curr. Opin. Microbiol.* **59**, 42–49 (2021).
24. Malireddi, R. K., Ippagunta, S., Lamkanfi, M. & Kanneganti, T. D. Cutting edge: proteolytic inactivation of poly(ADP-ribose) polymerase 1 by the Nlrp3 and Nlrc4 inflammasomes. *J. Immunol.* **185**, 3127–3130 (2010).
25. Lamkanfi, M. et al. Targeted peptidocentric proteomics reveals caspase-7 as a substrate of the caspase-1 inflammasomes. *Mol. Cell Proteomics* **7**, 2350–2363 (2008).
26. Lukens, J. R. et al. Dietary modulation of the microbiome affects autoinflammatory disease. *Nature* **516**, 246–249 (2014).
27. Gurung, P. et al. FADD and caspase-8 mediate priming and activation of the canonical and noncanonical Nlrp3 inflammasomes. *J. Immunol.* **192**, 1835–1846 (2014).
28. Karki, R. et al. Synergism of TNF- α and IFN- γ triggers inflammatory cell death, tissue damage, and mortality in SARS-CoV-2 infection and cytokine shock syndromes. *Cell* **184**, 149–168.e117 (2021).
29. Malireddi, R. K. S. et al. Innate immune priming in the absence of TAK1 drives RIPK1 kinase activity-independent pyroptosis, apoptosis, necroptosis, and inflammatory disease. *J. Exp. Med.* **217**, e20191644 (2020).
30. Malireddi, R. K. S. et al. TAK1 restricts spontaneous NLRP3 activation and cell death to control myeloid proliferation. *J. Exp. Med.* **215**, 1023–1034 (2018).
31. Zheng, M., Karki, R., Vogel, P. & Kanneganti, T. D. Caspase-6 is a key regulator of innate immunity, inflammasome activation, and host defense. *Cell* **181**, 674–687.e613 (2020).
32. Banerjee, I. et al. Gasdermin D restrains type I interferon response to cytosolic DNA by disrupting ionic homeostasis. *Immunity* **49**, 413–426.e415 (2018).
33. Christgen, S. et al. Identification of the PANoptosome: a molecular platform triggering pyroptosis, apoptosis, and necroptosis (PANoptosis). *Front. Cell Infect. Microbiol.* **10**, 237 (2020).
34. Sharma, D., Malik, A., Guy, C., Vogel, P. & Kanneganti, T. D. TNF/TNFR axis promotes pyrin inflammasome activation and distinctly modulates pyrin inflammasomopathy. *J. Clin. Invest.* **129**, 150–162 (2019).
35. Jones, J. W. et al. Absent in melanoma 2 is required for innate immune recognition of *Francisella tularensis*. *Proc. Natl Acad. Sci. USA* **107**, 9771–9776 (2010).
36. Henry, T., Brotcke, A., Weiss, D. S., Thompson, L. J. & Monack, D. M. Type I interferon signaling is required for activation of the inflammasome during *Francisella* infection. *J. Exp. Med.* **204**, 987–994 (2007).

Publisher's note Springer Nature remains neutral with regard to jurisdictional claims in published maps and institutional affiliations.

© The Author(s), under exclusive licence to Springer Nature Limited 2021

Article

Methods

Mice

C57BL/6J (wild type), *Mefv*^{-/-} (ref. 21), *Aim2*^{-/-} (ref. 34), *Nlrp3*^{-/-} (ref. 37), *Nlrp4*^{-/-} (ref. 38), *Zbp1*^{-/-} (ref. 39), *Tlr3*^{-/-} (ref. 40), *Trif*^{-/-} (ref. 41), *Mdas5*^{-/-} (ref. 42), *Mavs*^{-/-} (ref. 43), *Nlrp6*^{-/-} (ref. 44), *Nlrp12*^{-/-} (ref. 45), *Asc*^{-/-} (ref. 46), *Casp1*^{-/-} (ref. 47), *Casp1*^{C284A/C284A} (ref. 48), *Gsdmd*^{-/-} (ref. 49), *Casp8*^{DA/DA} (ref. 50), *Casp7*^{-/-} (ref. 51), *Casp3*^{-/-} (ref. 52), *Casp6*^{-/-} (Jackson Laboratory, 006236; ref. 31), *Ripk3*^{-/-} (ref. 53), *Ripk3*^{-/-} *Casp8*^{-/-} (ref. 54) and *Ripk3*^{-/-} *Fadd*^{-/-} (ref. 55) mice have been described previously. *Mefv*^{-/-} mice were crossed with *Zbp1*^{-/-} mice to generate *Mefv*^{-/-} *Zbp1*^{-/-} homozygous knockouts. All mice were bred and maintained in a specific pathogen-free facility at the Animal Resource Center at St. Jude Children's Research Hospital and were backcrossed to the C57BL/6 background (J substrain) for at least 10 generations. Both male and female mice were used in this study; age- and sex-matched 6- to 8-week-old mice were used for in vivo and 6- to 12-week-old mice were used for in vitro studies. Cohoused mice were used for in vivo analyses. Mice were maintained in 20–23.3 °C and 30–70% humidity with a 12 h light/dark cycle and were fed standard chow. Animal studies were conducted under protocols approved by the St. Jude Children's Research Hospital committee on the Use and Care of Animals.

Cell culture

Primary BMDMs were cultivated for 6 days in DMEM (Thermo Fisher Scientific, 12440-053) supplemented with 10% FBS (Biowest, S1620), 30% L929-conditioned medium, 1% non-essential amino acids (Thermo Fisher Scientific, 11140-050) and 1% penicillin and streptomycin (Thermo Fisher Scientific, 15070-063). BMDMs were then seeded into 12-well plates at a density of 1 million cells per well and incubated overnight before use. THP-1 cells (ATCC TIB-202) were grown in RPMI 1640 with 10% FBS and differentiated into macrophages in RPMI 1640 medium containing 20% FBS and 100 ng ml⁻¹ phorbol 12-myristate 13-acetate (PMA) for 2 days. The THP-1 cell line was purchased directly from ATCC and was not further authenticated in our laboratory. Cells were tested for mycoplasma contamination using mycoplasma detection PCR and were found to be negative for mycoplasma contamination.

Virus and bacteria culture

Human herpes simplex virus 1 (HF strain) (ATCC; VR-260) was propagated in Vero cells, and the virus titre was measured by plaque assay in Vero cells. The influenza A virus (A/Puerto Rico/8/34, H1N1 (PR8)) was prepared as previously described³¹ and propagated from 11-day-old embryonated chicken eggs by allantoic inoculation. Influenza A virus titre was measured by plaque assay in MDCK cells. *Salmonella* Typhimurium strain SL1344 was inoculated into Luria-Bertani (LB) broth (MP Biomedicals, 3002-031) and incubated overnight under aerobic conditions at 37 °C. *S. Typhimurium* was then sub-cultured (1:10) for 3 h at 37 °C in fresh LB broth to generate bacteria grown to log phase. *C. difficile* strain r20291 AB⁻ and AB⁺ strains (provided by N. Minton⁵⁶) were streaked onto brain heart infusion agar (BD Biosciences, 211065) and incubated overnight at 37 °C in an anaerobic chamber. Single colonies were inoculated into tryptone-yeast extract medium and grown overnight at 37 °C anaerobically. *F. novicida* strain U112 was prepared as previously described⁶ and was grown in BBL Trypticase Soy Broth (TSB) (211768, BD Biosciences) supplemented with 0.2% L-cysteine (Fisher) overnight under aerobic conditions at 37 °C. Bacteria were subcultured (1:10) in fresh TSB supplemented with 0.2% L-cysteine for 3 h and resuspended in PBS. Gentamicin (50 µg ml⁻¹, Gibco) was added 3 h after infection to kill extracellular *F. novicida*.

Cell stimulation and infection

For ligand-mediated AIM2 inflammasome activation, 2 µg of poly(dA:dT) (InvivoGen, tlr1-patn) was resuspended in PBS and mixed with 0.6 µl of Xfect polymer in Xfect reaction buffer (Clontech Laboratories, 631318). After 10 min, DNA complexes were added to

BMDMs in Opti-MEM (ThermoFisher Scientific, 31985-070), followed by incubation for 5 h. For NLRP3 inflammasome activation, BMDMs were primed for 4 h with 500 ng ml⁻¹ ultrapure lipopolysaccharide (LPS) from *Escherichia coli* (O111:B4) (Invivogen, tlr1-3pelps) and then stimulated for 45 min with 20 µM nigericin (Sigma, N7143). For NLRP4 inflammasome activation, *S. Typhimurium* was infected at an MOI of 1 for 2 h. For pyrin inflammasome activation, toxin AB⁺ *C. difficile* (2 × 10⁷ colony-forming units (CFU) ml⁻¹) were spun down, and the supernatant was sterilized using 0.22 µm filters and then added to BMDMs for 12 h. For HSV1 (6, 12 or 16 h; MOI 10) and IAV (16 h; MOI 10) infections, cells were infected in DMEM plain medium (Sigma, D6171). For *F. novicida* infection, cells were infected in DMEM (ThermoFisher Scientific, 11995-065) at a MOI of 50 (12 or 16 h) to determine caspase, GSDMD, and GSDME cleavage and for cell death analyses, at a MOI of 150 (24 h) to determine phosphorylated MLKL and RIPK3 levels or at a MOI of 1 (3 h) for IFN analyses. For inhibition of the pyrin inflammasome, 30 µM colchicine (Sigma, C9754) was added to BMDMs 1 h before infection. For inhibition of caspase-1, 20 µM VX-765 (Chemietek, CT-VX765) was added to BMDMs 1 h before the infection. For the IFN-β treatment, 50 ng ml⁻¹ of IFN-β (PBL Assay, 12400-1) was added to BMDMs 3 h after infections. To measure in vitro viral titre, the indicated BMDMs were infected with HSV1 (MOI 10) for 12 h, and the supernatants were used for plaque assays in Vero cells. To measure in vitro *F. novicida* levels, cells were infected at an MOI of 100, and cells were collected with PBS containing 0.5% Triton X-100 at 6 or 12 h after infection. The *F. novicida* were then streaked onto TSB plates supplemented with 0.2% L-cysteine and grown overnight at 37 °C anaerobically.

siRNA-mediated gene silencing

The Accell human siRNA SMART Pools against *AIM2* (E-011951-00-0010), *MEFV* (E-011081-00-0010) and *ZBP1* (E-014650-00-0010) genes were purchased from Horizon. THP-1 macrophages were transfected with siRNA using Accell siRNA delivery media according to the manufacturer's instructions (Horizon). As a negative control, non-targeting control siRNA (D-001910-01-50) was used.

Real-time PCR analysis

RNA was extracted using TRIzol according to the manufacturer's instructions (Life Technologies). Isolated RNA was reverse transcribed to cDNA using the First-Strand cDNA Synthesis Kit (Life Technologies). Real-time PCR was performed on an ABI 7500 real-time PCR instrument with 2× SYBR Green (Applied Biosystems). Primer sequences used in this study were as follows: 5'-AAGAGTCCCCTGCGATTATTTG-3' and 5'-TCTGGATGGCGTTTGAATTGG-3' for *Zbp1*; 5'-TCATCTGCTAAAC ACCCTGGA-3' and 5'-GGGATCTTAGAGTGGCCCTTC-3' for *Mefv*; 5'-CGTCCGTAGACAAAATGGT-3' and 5'-TTGATGGCAACAATCTCCAC-3' for *Gapdh*.

Measurement of active RhoA-GTP levels

BMDMs (2 × 10⁶ cells) were seeded in 6-well plates and transfected with 0.5 µg ml⁻¹ TcdB, 0.5 µg poly(dA:dT) or infected with HSV (MOI 10) or *F. novicida* (MOI 100). RhoA-GTP levels were measured using the RhoA G-LISA Activation Assay kit (BK121, Cytoskeleton) and normalized to total RhoA levels, which were measured using the Total RhoA ELISA kit (BK150, Cytoskeleton) according to the manufacturer's instructions. For pull-down assays, a GST-tagged Rho binding domain (RBD) in the Rho effector protein was used, which has been shown to bind specifically to the GTP-bound form of RhoA^{17,19}. RhoA-GTP in BMDMs (2 × 10⁶ cells) was pull-down with Rhotekin-RBD beads using the RhoA activation Assay Biochem Kit (BK036, Cytoskeleton) according to the manufacturer's instructions.

In vivo infection

Age- and sex-matched, 6- to 8-week-old wild-type wild-type and *Aim2*^{-/-}, *Mefv*^{-/-} and *Zbp1*^{-/-} mice were used for infections. For HSV1 infection,

mice were anaesthetized with 250 mg kg⁻¹ avertin and then infected intranasally with HSV1 in 50 µl PBS containing around 5 × 10⁷ PFU. Infected mice were monitored over a period of 14 days for survival. For the *F. novicida* infection, *F. novicida* strain U112 was grown in TSB supplemented with 0.2% L-cysteine overnight at 37 °C and then 1:10 subcultured for 4 h before infection. Mice were infected subcutaneously with 5 × 10⁵ CFU of *F. novicida* in 200 µl PBS. Infected mice were monitored over a period of 12 days for survival. Lungs, livers and/or spleens collected at the indicated time points were homogenized in 1 ml PBS for viral titres to be enumerated by plaque assays or for bacterial titres to be streaked onto TSB supplemented with 0.2% L-cysteine plates and grown overnight at 37 °C anaerobically.

Immunoblot analysis

Immunoblotting was performed as described previously⁵⁷. In brief, for caspase analysis, BMDMs were lysed along with the supernatant using 50 µl caspase lysis buffer (1× protease inhibitors, 1× phosphatase inhibitors, 10% NP-40 and 25 mM DTT) followed by the addition of 100 µl 4× SDS loading buffer. For signalling analysis, the BMDM supernatants were removed at the indicated time points, and cells were washed once with PBS, after which cells were lysed with RIPA buffer. Proteins from lung, spleen and liver tissues were extracted using RIPA buffer supplemented with protease and phosphatase inhibitors (Roche), and 30 µg per sample was loaded on the gel. Proteins were separated by electrophoresis through 8%–12% polyacrylamide gels. Following electrophoretic transfer of proteins onto PVDF membranes (Millipore, IPVH00010), non-specific binding was blocked by incubation with 5% skim milk; then membranes were incubated with the following primary antibodies: anti-caspase-1 (AdipoGen, AG-20B-0042, 1:1,000), anti-caspase-3 (CST, 9662, 1:1,000), anti-cleaved caspase-3 (CST, 9661, 1:1,000), anti-caspase-7 (CST, 9492, 1:1,000), anti-cleaved caspase-7 (CST, 9491, 1:1,000), anti-caspase-8 (CST, 4927, 1:1,000), anti-cleaved caspase-8 (CST, 8592, 1:1,000), anti-pRIPK3 (CST, 91702 S, 1:1,000), anti-RIPK3 (ProSci, 2283, 1:1,000), anti-pMLKL (CST, 37333, 1:1,000), anti-MLKL (Abgent, AP14272b, 1:1,000), anti-GSDMD (Abcam, ab209845, 1:1,000), anti-GSDME (Abcam, ab215191, 1:1,000), anti-pyruvate kinase (Abcam, ab195975, 1:1,000), anti-AIM2 (Abcam, ab119791, 1:1,000), anti-ZBP1 (AdipoGen, AG-20B-0010, 1:1,000), anti-ASC (Millipore, 04-147, 1:1,000 or AdipoGen, AG-25B-006-C100, 1:1,000), anti-RIPK1 (CST, 3493, 1:1,000), anti-FADD (Millipore, 05-486, 1:1,000), anti-β-actin (Proteintech, 66009-1-IG, 1:5,000), human anti-caspase-1 (R&D systems, MAB6215, 1:1,000), human anti-β-actin (CST, 4970, 1:1,000). Membranes were then washed and incubated with the appropriate horseradish peroxidase (HRP)-conjugated secondary antibodies (1:5,000 dilution; Jackson Immuno Research Laboratories, anti-rabbit (111-035-047), anti-mouse (315-035-047)) for 1 h. Proteins were visualized by using Luminata Forte Western HRP Substrate (Millipore, WBLUF0500), and membranes were developed with an Amersham imager; images were analysed with ImageJ (v1.53a).

Real-time cell death analysis

Real-time cell death assays were performed using an InCuCyte S3 imaging system (Essen Biosciences). BMDMs or THP-1 cells were seeded in 12-well plates (10⁶ BMDMs or 5 × 10⁵ THP-1 cells per well) and stimulated. After infection, 100 nM SYTOX Green (Thermo Fisher Scientific, S7020) was added. The images were acquired every 1 h at 37 °C and 5% CO₂. The resulting images were analysed using the software package supplied with the InCuCyte imager, which counts the number of Sytox Green-positive BMDM nuclei (Sytox⁺ BMDM nuclei) present in each image.

Immunoprecipitation

Immunoprecipitation was performed as described previously⁵⁸. In brief, after HSV1 or *F. novicida* infection or poly(dA:dT) treatment, wild-type BMDMs were lysed in a buffer containing 20 mM Tris-HCl

(pH 7.4), 100 mM NaCl, 30 mM KCl and 0.1% NP-40. After centrifugation at 16,000g for 10 min, the lysates were incubated with either IgG control antibody (CST, 3900 S) or anti-ASC antibody (AdipoGen; AG-25B-006-C100) with protein A/G PLUS-Agarose (Santa Cruz Biotechnology) overnight at 4 °C. After washing with the above buffer, the immunoprecipitated proteins were collected by boiling in 1× SDS loading buffer at 100 °C for 5 min.

Immunofluorescence staining

Immunofluorescence staining was performed as described previously⁵⁹. In brief, after infection, BMDMs were fixed in 4% paraformaldehyde (ChemCruz, sc-281692) for 10 min and permeabilized with PBS containing 0.5% Triton X-100 for 3 min. Cells were then incubated in PBS containing 1% skim milk for 1 h. Alexa Fluor 488 (ThermoFisher, A20181)-conjugated anti-ASC (Millipore, 04-147), Alexa Fluor 532 (ThermoFisher, A20182)-conjugated anti-AIM2 (Abcam, ab119791), Alexa Fluor 568 (ThermoFisher, A20184)-conjugated anti-pyruvate kinase (Abcam, ab195975), Alexa Fluor 647 (ThermoFisher, A20186)-conjugated anti-ZBP1 (AdipoGen, AG-20B-0010), Alexa Fluor 568 (ThermoFisher, A20184)-conjugated anti-RIPK3 (ProSci, 2283) or Alexa Fluor 647 (ThermoFisher, A20186)-conjugated anti-caspase-8 (Enzo, IG12) were made according to the manufacturer's instructions, and the coverslips were incubated with indicated antibodies (1:100) for 1 h. Cells were counterstained with DAPI mounting medium (Invitrogen, P36931). Images were acquired by confocal laser scanning microscopy (LSM780; Carl Zeiss) using 63× Apochromat objective.

Cytokine analysis

Cytokines were detected by using multiplex ELISA (Millipore, MCYTOMAG-70K), IL-18 ELISA (Invitrogen, BMS618-3) or IFN-β ELISA (BioLegend, 439408) according to the manufacturer's instructions.

Statistical analysis

GraphPad Prism 8.0 software was used for data analysis. Data are presented as mean ± s.e.m. Statistical significance was determined by *t*-tests (two-tailed) for two groups or one-way ANOVA with Dunnett's multiple comparisons test for more groups. Survival analysis was performed using the log-rank (Mantel-Cox) test. *P* values less than 0.05 were considered statistically significant where, **P* < 0.05, ***P* < 0.01, ****P* < 0.001 and *****P* < 0.0001.

Reporting summary

Further information on research design is available in the Nature Research Reporting Summary linked to this paper.

Data availability

The datasets generated and analysed during the current study are contained within the manuscript and the accompanying extended data figures. Source data are provided with this paper.

37. Kanneganti, T. D. et al. Bacterial RNA and small antiviral compounds activate caspase-1 through cryopyrin/Nalp3. *Nature* **440**, 233–236 (2006).
38. Mariathasan, S. et al. Differential activation of the inflammasome by caspase-1 adaptors ASC and Ipaf. *Nature* **430**, 213–218 (2004).
39. Ishii, K. J. et al. TANK-binding kinase-1 delineates innate and adaptive immune responses to DNA vaccines. *Nature* **451**, 725–729 (2008).
40. Alexopoulou, L., Holt, A. C., Medzhitov, R. & Flavell, R. A. Recognition of double-stranded RNA and activation of NF-κB by Toll-like receptor 3. *Nature* **413**, 732–738 (2001).
41. Yamamoto, M. et al. Role of adaptor TRIF in the MyD88-independent toll-like receptor signaling pathway. *Science* **301**, 640–643 (2003).
42. Gitlin, L. et al. Essential role of mda-5 in type I IFN responses to polyriboinosinic:polyribocytidylic acid and encephalomyocarditis picornavirus. *Proc. Natl. Acad. Sci. USA* **103**, 8459–8464 (2006).
43. Kumar, H. et al. Essential role of IPS-1 in innate immune responses against RNA viruses. *J. Exp. Med.* **203**, 1795–1803 (2006).
44. Chen, G. Y., Liu, M., Wang, F., Bertin, J. & Núñez, G. A functional role for Nlrp6 in intestinal inflammation and tumorigenesis. *J. Immunol.* **186**, 7187–7194 (2011).

45. Zaki, M. H. et al. The NOD-like receptor NLRP12 attenuates colon inflammation and tumorigenesis. *Cancer Cell* **20**, 649–660 (2011).
46. Ozören, N. et al. Distinct roles of TLR2 and the adaptor ASC in IL-1 β /IL-18 secretion in response to *Listeria monocytogenes*. *J. Immunol.* **176**, 4337–4342 (2006).
47. Man, S. M. et al. IRGB10 liberates bacterial ligands for sensing by the AIM2 and Caspase-11-NLRP3 inflammasomes. *Cell* **167**, 382–396.e317 (2016).
48. Van Opendenbosch, N. et al. Caspase-1 engagement and TLR-induced c-FLIP expression suppress ASC/Caspase-8-dependent apoptosis by inflammasome sensors NLRP1b and NLRP3. *Cell Rep.* **21**, 3427–3444 (2017).
49. Karki, R. et al. IRF8 regulates transcription of *Naips* for NLRP4 inflammasome activation. *Cell* **173**, 920–933.e913 (2018).
50. Tummers, B. et al. Caspase-8-dependent inflammatory responses are controlled by its adaptor, FADD, and necroptosis. *Immunity* **52**, 994–1006.e1008 (2020).
51. Lakhani, S. A. et al. Caspases 3 and 7: key mediators of mitochondrial events of apoptosis. *Science* **311**, 847–851 (2006).
52. Zheng, T. S. et al. Deficiency in caspase-9 or caspase-3 induces compensatory caspase activation. *Nat. Med.* **6**, 1241–1247 (2000).
53. Newton, K., Sun, X. & Dixit, V. M. Kinase RIP3 is dispensable for normal NF- κ Bs, signaling by the B-cell and T-cell receptors, tumor necrosis factor receptor 1, and Toll-like receptors 2 and 4. *Mol. Cell. Biol.* **24**, 1464–1469 (2004).
54. Oberst, A. et al. Catalytic activity of the caspase-8FLIP_L complex inhibits RIPK3-dependent necrosis. *Nature* **471**, 363–367 (2011).
55. Dillon, C. P. et al. Survival function of the FADD–CASPASE-8–cFLIP_L complex. *Cell Rep.* **1**, 401–407 (2012).
56. Kuehne, S. A. et al. Importance of toxin A, toxin B, and CDT in virulence of an epidemic *Clostridium difficile* strain. *J. Infect. Dis.* **209**, 83–86 (2014).
57. Tweedell, R. E., Malireddi, R. K. S. & Kanneganti, T. D. A comprehensive guide to studying inflammasome activation and cell death. *Nat. Protoc.* **15**, 3284–33339 (2020).
58. Lee, S. et al. Influenza restriction factor MxA functions as inflammasome sensor in the respiratory epithelium. *Sci. Immunol.* **4**, eaau4643 (2019).
59. Lee, S., Hirohama, M., Noguchi, M., Nagata, K. & Kawaguchi, A. Influenza A virus infection triggers pyroptosis and apoptosis of respiratory epithelial cells through the type I interferon signaling pathway in a mutually exclusive manner. *J. Virol.* **92**, e00396–18 (2018).

Acknowledgements We thank members of the Kanneganti laboratory for their comments and suggestions and R. Tweedell for scientific editing and writing support. *Mavs*^{-/-} mutant mice were kindly provided by M. Gale. We thank M. Yamamoto for the *Trif*^{-/-} mutant mouse strain. T.-D.K. is supported by NIH grants AI101935, AI124346, AI160179, AR056296 and CA253095 and by the American Lebanese Syrian Associated Charities. The content is solely the responsibility of the authors and does not necessarily represent the official views of the National Institutes of Health.

Author contributions S.L., R.K. and T.-D.K. conceptualized the study; S.L. and R.K. designed the methodology; S.L., R.K., Y.W., L.N.N. and R.C.K. performed the experiments; S.L., R.K., Y.W. and L.N.N. conducted the analysis; S.L., R.K. and T.-D.K. wrote the manuscript. T.-D.K. acquired the funding and provided overall supervision.

Competing interests The authors declare no competing interests.

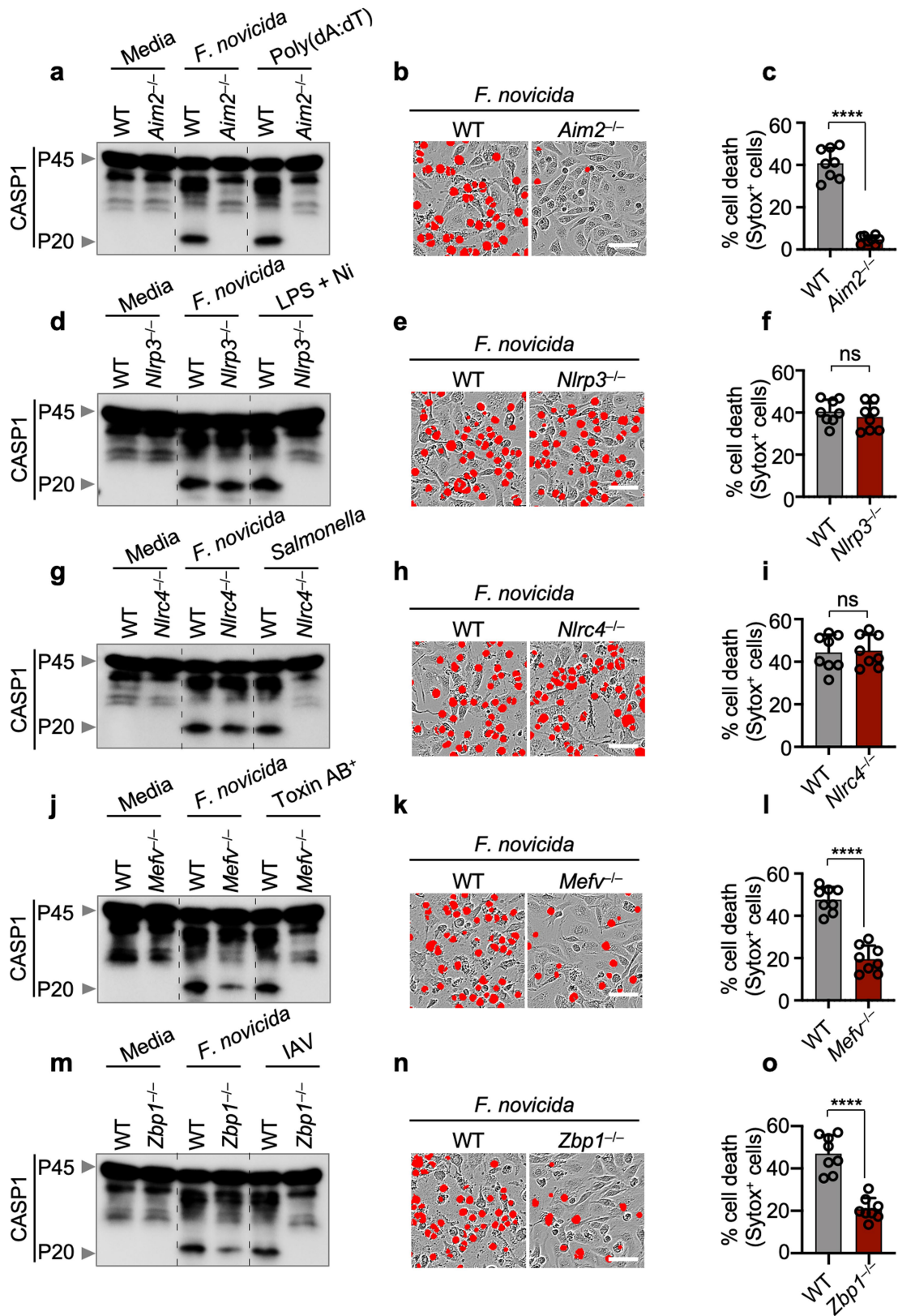
Additional information

Supplementary information The online version contains supplementary material available at <https://doi.org/10.1038/s41586-021-03875-8>.

Correspondence and requests for materials should be addressed to Thirumala-Devi Kanneganti.

Peer review information *Nature* thanks the anonymous reviewer(s) for their contribution to the peer review of this work.

Reprints and permissions information is available at <http://www.nature.com/reprints>.



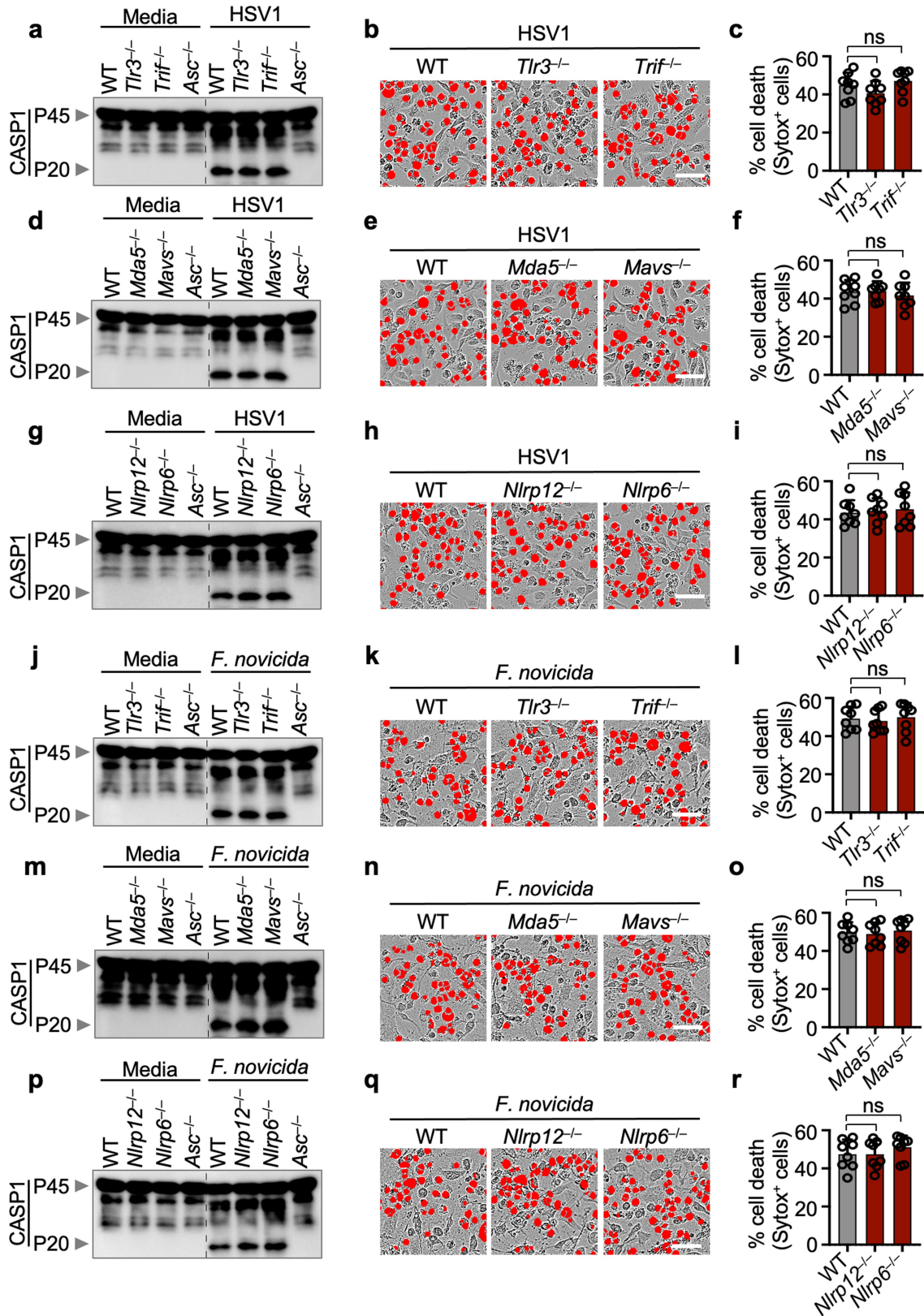
Extended Data Fig. 1 | See next page for caption.

Article

Extended Data Fig. 1 | *F. novicida* induces AIM2-, Pyrin-, ZBP1-mediated

caspace-1 activation, cytokine release and cell death. **a**, Immunoblot analysis of pro-caspase-1 (CASPI; P45) and cleaved CASPI (P20) in *F. novicida*-infected or poly(dA:dT)-transfected wild type (WT) or *Aim2*^{-/-} bone marrow-derived macrophages (BMDMs). **b**, Cell death in BMDMs after *F. novicida* infection for 16 h. Red indicates dead cells. **c**, Quantification of the cell death in **(b)**. **d–f**, Immunoblot analysis of CASPI (**d**), cell death images at 16 h post-infection (**e**), and cell death quantification (**f**) from WT or *Nlrp3*^{-/-} BMDMs after *F. novicida* infection or LPS plus nigericin (LPS + Ni) treatment. **g–i**, Immunoblot analysis of CASPI (**g**), cell death images at 16 h post-infection (**h**), and cell death quantification (**i**) from WT or *Nlrca4*^{-/-} BMDMs after *F. novicida* or *Salmonella* Typhimurium infection. **j–l**, Immunoblot analysis of CASPI

(**j**), cell death images at 16 h post-infection (**k**), and cell death quantification (**l**) from WT or *Mefv*^{-/-} BMDMs after *F. novicida* infection or *C. difficile* Toxin AB⁺ supernatant treatment. **m–o**, Immunoblot analysis of CASPI (**m**), cell death images at 16 h post-infection (**n**), and cell death quantification (**o**) from WT or *Zbp1*^{-/-} BMDMs after *F. novicida* or influenza A virus (IAV) infection. **a, d, g, j, m**, Data are representative of at least three independent experiments. **b, e, h, k, n**, Images are representative of at least three independent experiments. Scale bar, 50 μ m. **c, f, i, l, o**, Data are mean \pm s.e.m. ns, not significant; **** $P < 0.0001$ (two-tailed t-test; $n = 8$ from 4 biologically independent samples). Exact P values are presented in Supplementary Table 1. For gel source data, see Supplementary Figure 1.



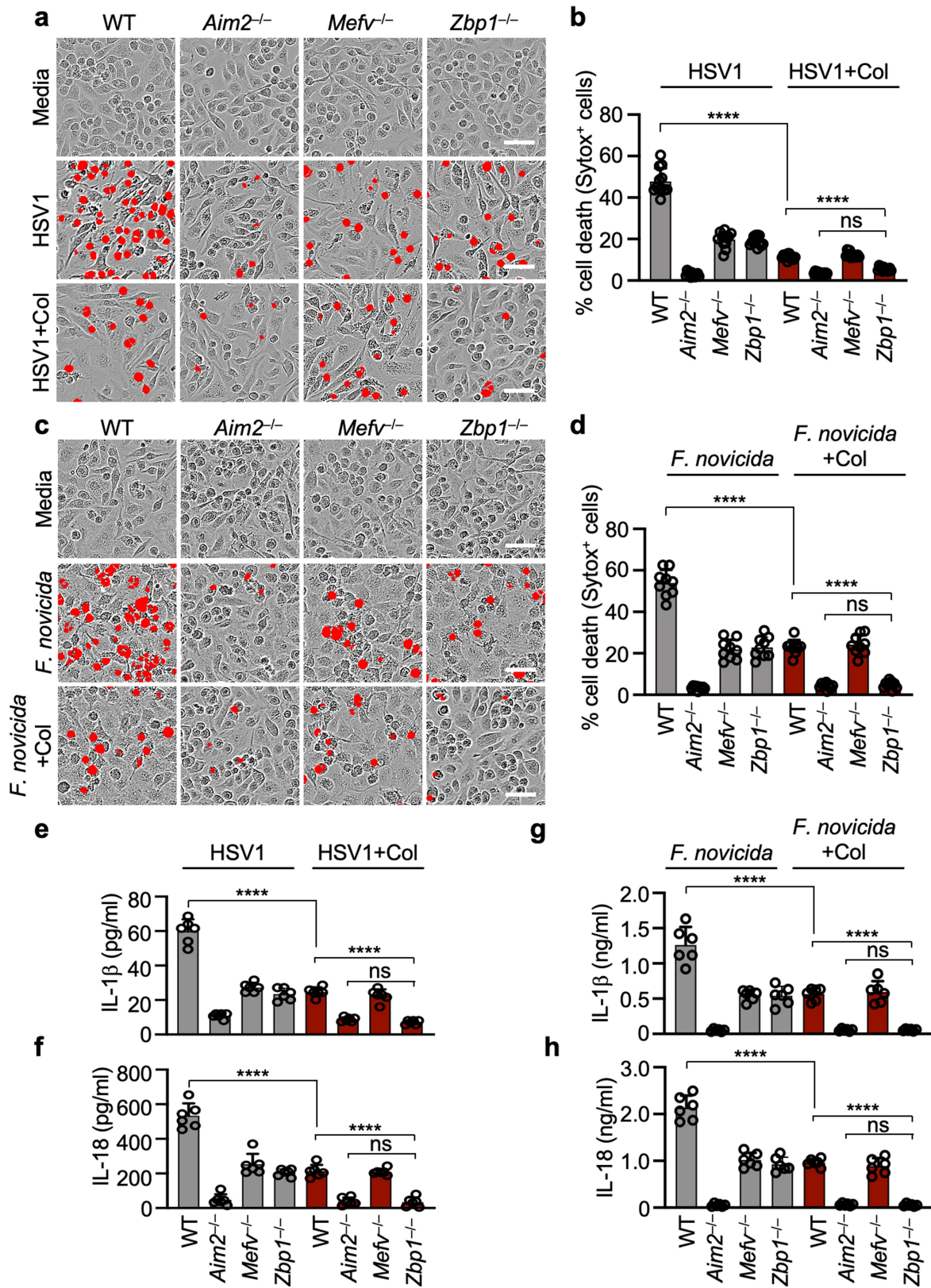
Extended Data Fig. 2 | See next page for caption.

Article

Extended Data Fig. 2 | Innate immune sensors TLR3, MDA5, NLRP6 and NLRP12 and adaptors Trif and MAVS are not required for caspase-1 activation and cell death after HSV1 and *F. novicida* infections.

a, Immunoblot analysis of pro-caspase-1 (CASP1; P45) and cleaved CASP1 (P20) in HSV1-infected wild type (WT), *Tlr3*^{-/-}, *Trif*^{-/-} or *Asc*^{-/-} bone marrow-derived macrophages (BMDMs). **b**, Cell death in BMDMs after HSV1 infection for 16 h. Red indicates dead cells. **c**, Quantification of the cell death in **(b)**. **d-f**, Immunoblot analysis of CASP1 (**d**), cell death images at 16 h post-infection (**e**), and cell death quantification (**f**) from WT, *Mda5*^{-/-} or *Mavs*^{-/-} BMDMs after HSV1 infection. **g-i**, Immunoblot analysis of CASP1 (**g**), cell death images at 16 h post-infection (**h**), and cell death quantification (**i**) from WT, *Nlrp6*^{-/-} or *Nlrp12*^{-/-} BMDMs after HSV1 infection. **j-l**, Immunoblot analysis of CASP1 (**j**), cell death

images at 16 h post-infection (**k**), and cell death quantification (**l**) from WT, *Tlr3*^{-/-} or *Trif*^{-/-} BMDMs after *F. novicida* infection. **m-o**, Immunoblot analysis of CASP1 (**m**), cell death images (**n**), and cell death quantification (**o**) from WT, *Mda5*^{-/-} or *Mavs*^{-/-} BMDMs after *F. novicida* infection. **p-r**, Immunoblot analysis of CASP1 (**p**), cell death images at 16 h post-infection (**q**), and cell death quantification (**r**) from WT, *Nlrp6*^{-/-} or *Nlrp12*^{-/-} BMDMs after *F. novicida* infection. **a, d, g, j, m, p**, Data are representative of at least three independent experiments. **b, e, h, k, n, q**, Images are representative of at least three independent experiments. Scale bar, 50 μ m. **c, f, i, l, o, r**, Data are mean \pm s.e.m. ns, not significant (one-way ANOVA with Dunnett's multiple comparisons test; $n = 8$ from 4 biologically independent samples). Exact *P* values are presented in Supplementary Table 1. For gel source data, see Supplementary Figure 1.

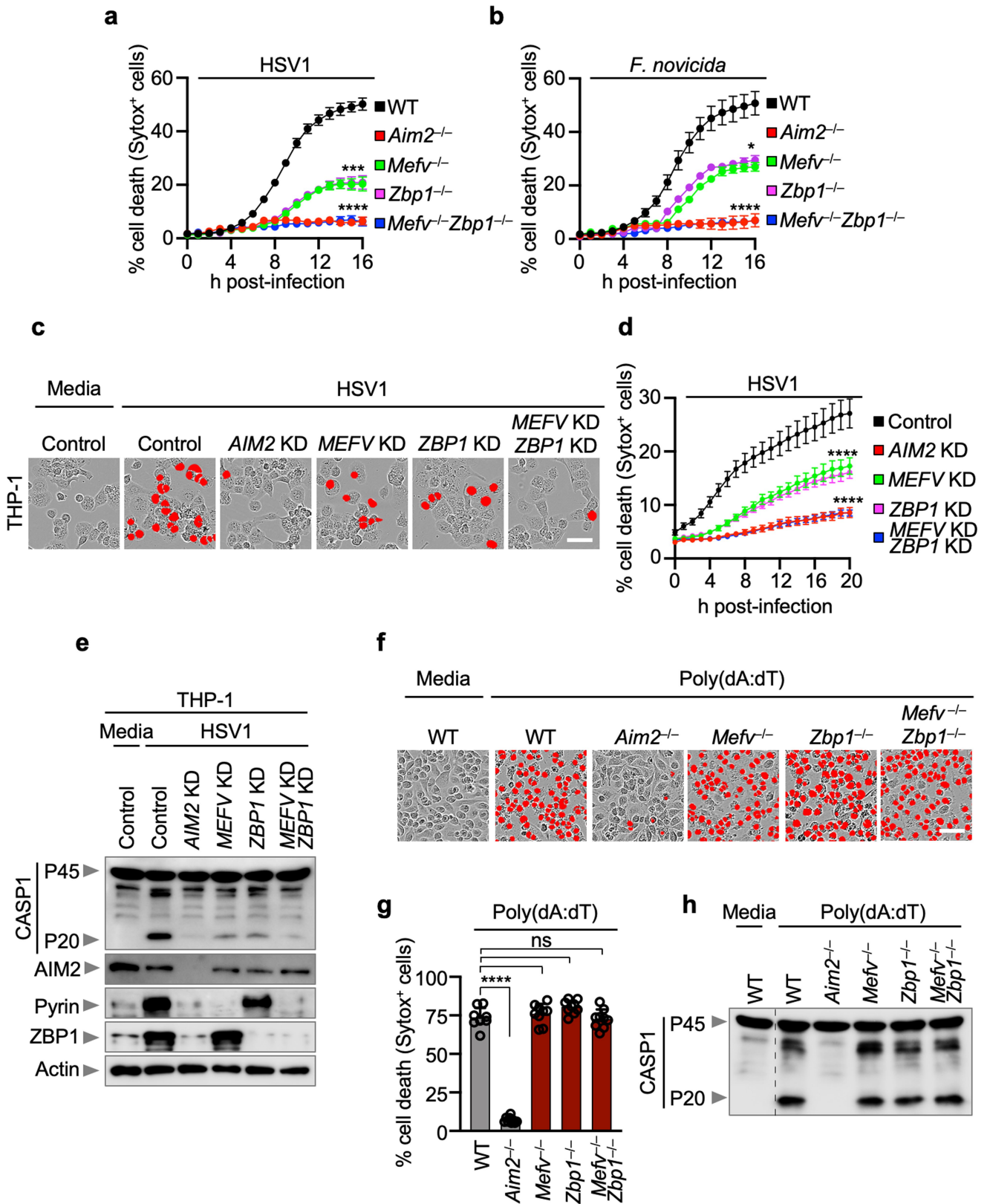


Extended Data Fig. 3 | See next page for caption.

Article

Extended Data Fig. 3 | ZBP1 cooperates with Pyrin to drive AIM2-mediated cell death and cytokine release. **a**, Cell death in bone marrow-derived macrophages (BMDMs) after HSV1 infection with or without colchicine (Col). Red indicates dead cells. Data are representative of at least three independent experiments. Scale bar, 50 μm . **b**, Quantification of the cell death from **(a)**. Data are mean \pm s.e.m. ns, not significant; **** $P < 0.0001$ (one-way ANOVA with Dunnett's multiple comparisons test; $n = 12$ from 3 biologically independent samples). **c**, Cell death in BMDMs after *F. novicida* infection with or without Col. Red indicates dead cells. Data are representative of at least three independent

experiments. Scale bar, 50 μm . **d**, Quantification of the cell death from **(c)**. Data are mean \pm s.e.m. ns, not significant; **** $P < 0.0001$ (one-way ANOVA with Dunnett's multiple comparisons test; $n = 9$ from 3 biologically independent samples). **e-h**, Release of IL-1 β (**e, g**) or IL-18 (**f, h**) following HSV1 (**e, f**) or *F. novicida* (**g, h**) infections with or without Col. Data are mean \pm s.e.m. ns, not significant; **** $P < 0.0001$ (one-way ANOVA with Dunnett's multiple comparisons test; $n = 6$ from 3 biologically independent samples). Exact P values are presented in Supplementary Table 1.



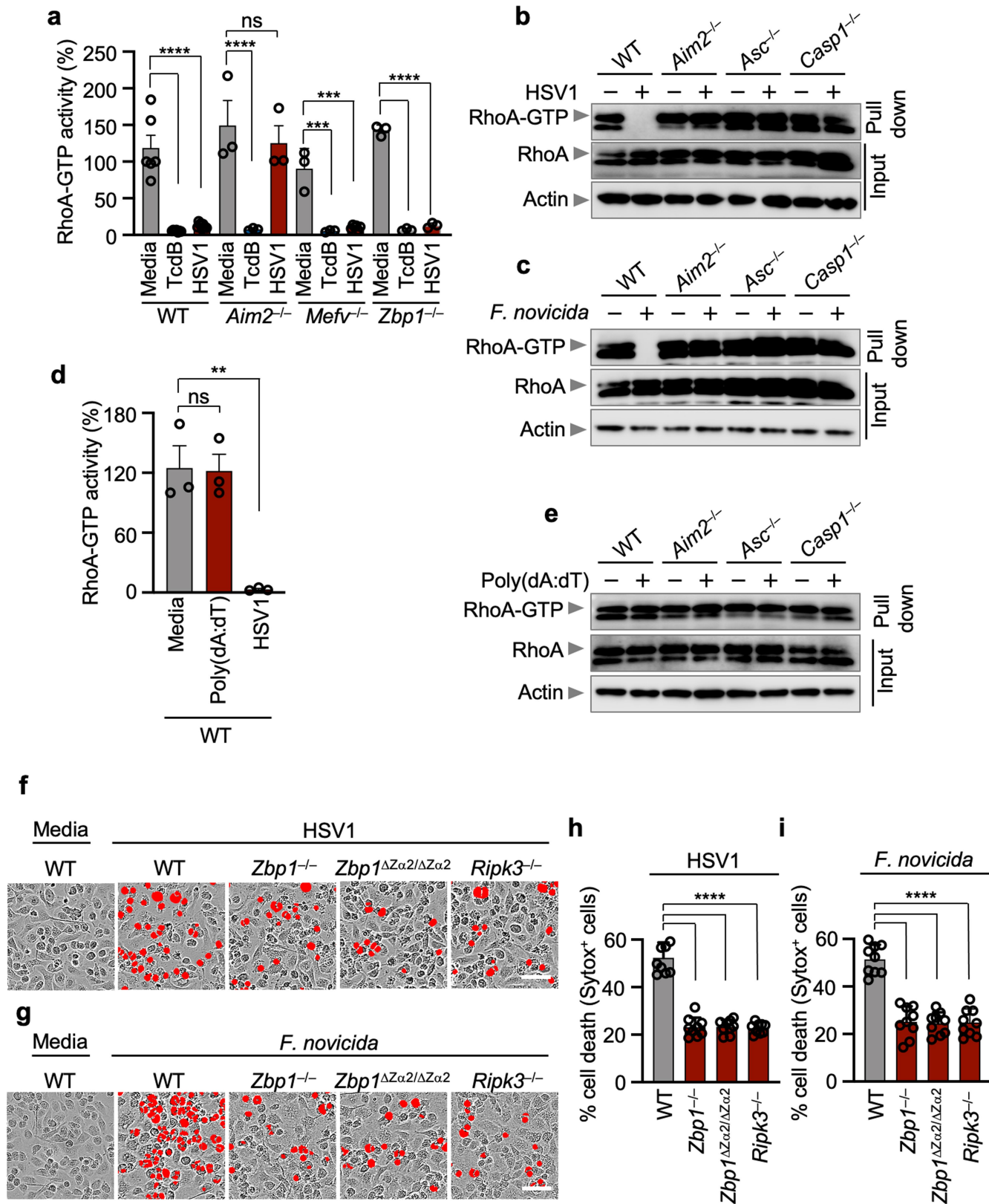
Extended Data Fig. 4 | See next page for caption.

Article

Extended Data Fig. 4 | Pyrin and ZBP1 are required for AIM2-mediated cell death following HSV1 infection, but not in response to poly(dA:dT).

a, b, Quantification of cell death in wild type (WT), *Aim2*^{-/-}, *Mefv*^{-/-}, *Zbp1*^{-/-} or *Mefv*^{-/-}*Zbp1*^{-/-} bone marrow-derived macrophages (BMDMs) over time during HSV1 (**a**) and *F. novicida* (**b**) infections. Data are mean ± s.e.m. **P* < 0.05; ****P* < 0.001; *****P* < 0.0001 (one-way ANOVA with Dunnett's multiple comparisons test; *n* = 4). Data are representative of at least three independent experiments. **c**, Cell death in THP-1 macrophages treated with control siRNA (Control) or siRNA targeted to *AIM2* (*AIM2* KD), *MEFV* (*MEFV* KD) and/or *ZBP1* (*ZBP1* KD) after HSV1 infection. Red indicates dead cells. Images are representative of at least three independent experiments. Scale bar, 50 μm. **d**, Quantification of the cell death from (**c**). Data are mean ± s.e.m. *****P* < 0.0001 (one-way ANOVA with Dunnett's multiple comparisons test;

n = 4). Data are representative of at least three independent experiments. **e**, Immunoblot analysis of caspase-1 (CASP1) activation and AIM2, Pyrin and ZBP1 expression in the indicated THP-1 cells. Data are representative of two independent experiments. **f**, Cell death in WT, *Aim2*^{-/-}, *Mefv*^{-/-}, *Zbp1*^{-/-} or *Mefv*^{-/-}*Zbp1*^{-/-} BMDMs after poly(dA:dT) transfection. Red indicates dead cells. Images are representative of at least three independent experiments. Scale bar, 50 μm. **g**, Quantification of the cell death from (**f**). Data are mean ± s.e.m. ns, not significant; *****P* < 0.0001 (one-way ANOVA with Dunnett's multiple comparisons test; *n* = 9 from 3 biologically independent samples). Exact *P* values are presented in Supplementary Table 1. **h**, Immunoblot analysis of CASP1 in the indicated BMDMs after poly(dA:dT) transfection. Data are representative of at least three independent experiments. For gel source data, see Supplementary Figure 1.



Extended Data Fig. 5 | See next page for caption.

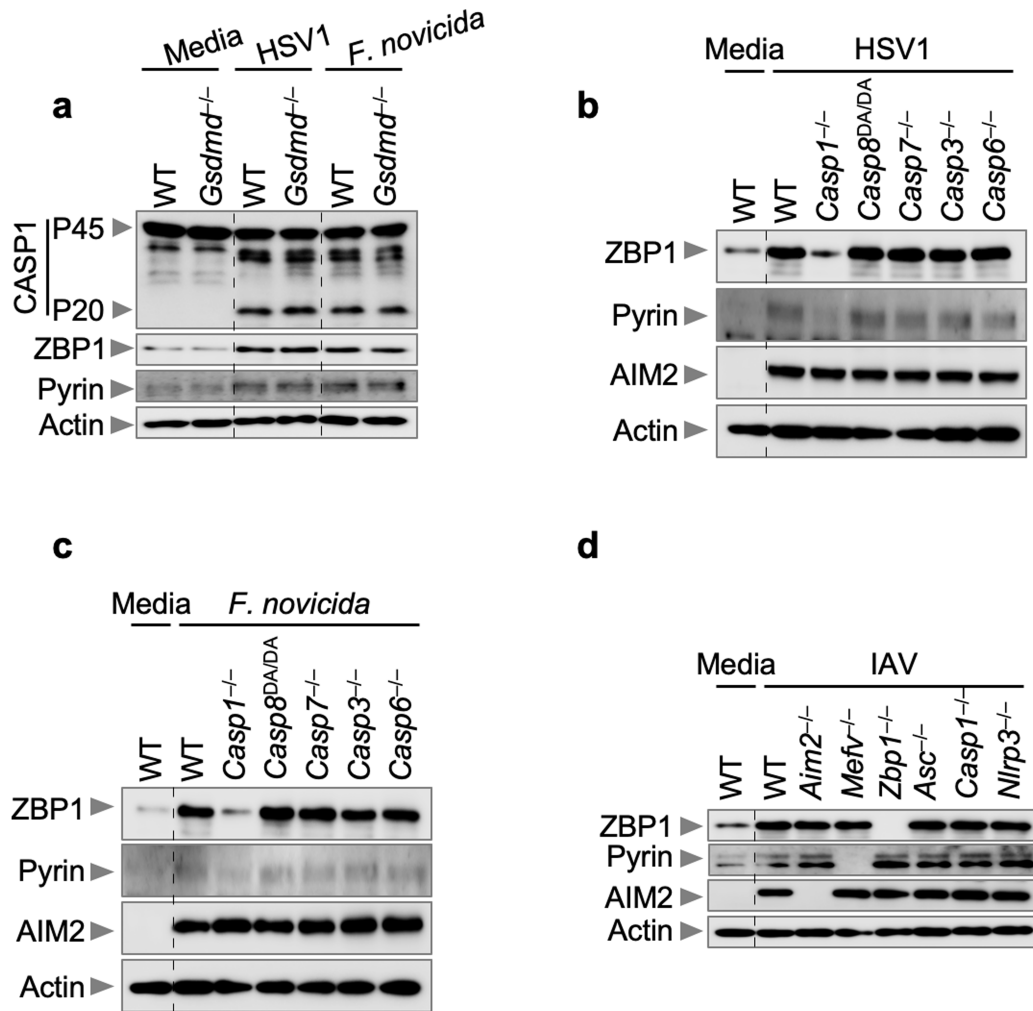
Article

Extended Data Fig. 5 | AIM2 acts as an upstream regulator of RhoA modifications, and the ZBP1 Z α 2 domain is required for cell death.

a, RhoA-GTP activity in wild type (WT), *Aim2*^{-/-}, *Mefv*^{-/-} or *Zbp1*^{-/-} bone marrow-derived macrophages (BMDMs) infected with HSV1 or treated with TcdB for 12 h. Activity was normalized to total RhoA levels. Data are mean \pm s.e.m. from three independent experiments. ns, not significant; ****P* < 0.001; *****P* < 0.0001 (one-way ANOVA with Dunnett's multiple comparisons test; *n* = 3, 6, 7 or 9).

b, c, Activated RhoA (RhoA-GTP) assessed using a pull-down assay with Rhotekin-RBD beads from WT, *Aim2*^{-/-}, *Asc*^{-/-} or *Casp1*^{-/-} BMDMs infected with HSV1 (**b**) or *F. novicida* (**c**). Data are representative of at least three independent experiments. **d**, RhoA-GTP activity in WT BMDMs infected with HSV1 or transfected with poly(dA:dT) for 12 h. Data are mean \pm s.e.m. from three

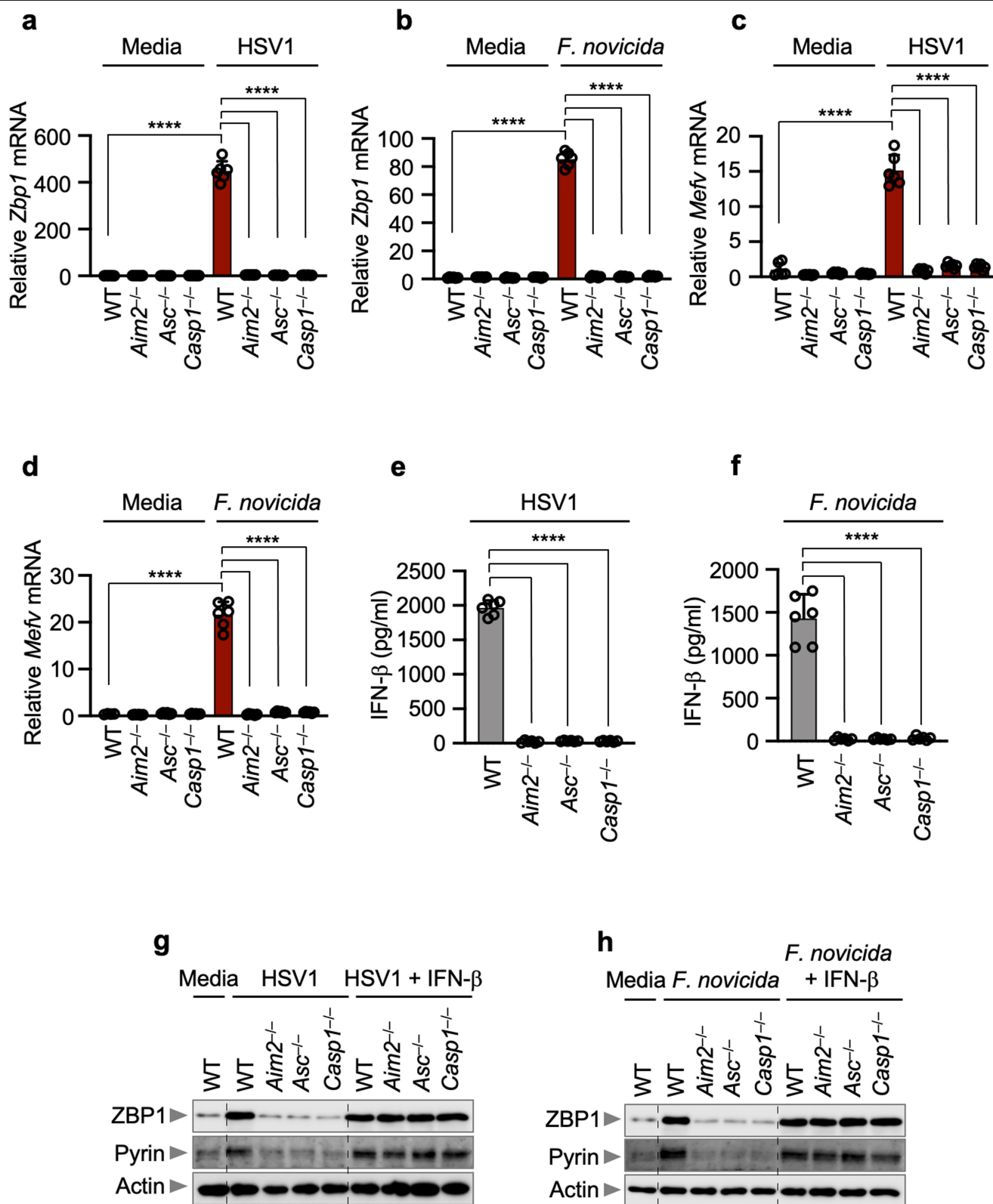
independent experiments. ns, not significant; ***P* < 0.01 (one-way ANOVA with Dunnett's multiple comparisons test; *n* = 3). **e**, Activated RhoA (RhoA-GTP) assessed using a pull-down assay with Rhotekin-RBD beads from WT, *Aim2*^{-/-}, *Asc*^{-/-} or *Casp1*^{-/-} BMDMs transfected with poly(dA:dT). Data are representative of at least three independent experiments. **f, g** Cell death in WT, *Zbp1*^{-/-}, *Zbp1* ^{Δ Z α 2/ Δ Z α 2} or *Ripk3*^{-/-} BMDMs after HSV1 (**f**) or *F. novicida* (**g**) infections. Red indicates dead cells. Images are representative of at least three independent experiments. Scale bar, 50 μ m. **h, i**, Quantification of the cell death from **f** (**h**) or **g** (**i**). Data are mean \pm s.e.m. *****P* < 0.0001 (one-way ANOVA with Dunnett's multiple comparisons test; *n* = 9 from 3 biologically independent samples). Exact *P* values are presented in Supplementary Table 1. For gel source data, see Supplementary Figure 1.



Extended Data Fig. 6 | The expression of Pyrin and ZBP1 is not regulated by GSDMD or caspase-8, -7, -3 or -6 during HSV1 or *F. novicida* infections.

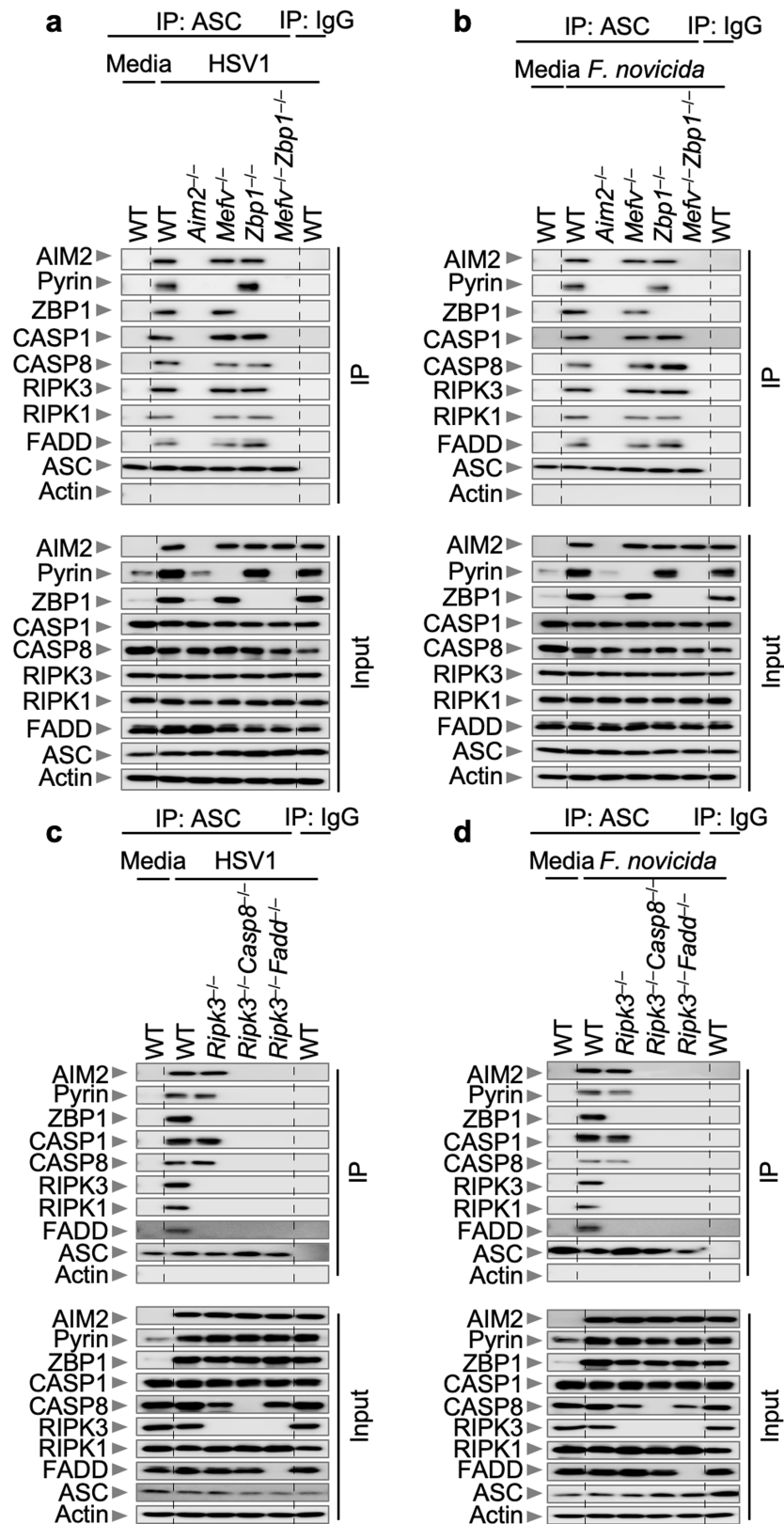
a, Immunoblot analysis of caspase-1 (CASP1) activation and ZBP1 and Pyrin expression in wild type (WT) or *Gsdmd*^{-/-} bone marrow-derived macrophages (BMDMs) after HSV1 or *F. novicida* infection. Data are representative of at least three independent experiments. **b, c**, Immunoblot analysis of ZBP1, Pyrin and

AIM2 expression in the indicated BMDMs after HSV1 (**b**) or *F. novicida* (**c**) infections. Data are representative of at least three independent experiments. **d**, Immunoblot analysis of ZBP1, Pyrin and AIM2 expression in the indicated BMDMs after influenza A virus (IAV) infection. Data are representative of at least three independent experiments. For gel source data, see Supplementary Figure 1.



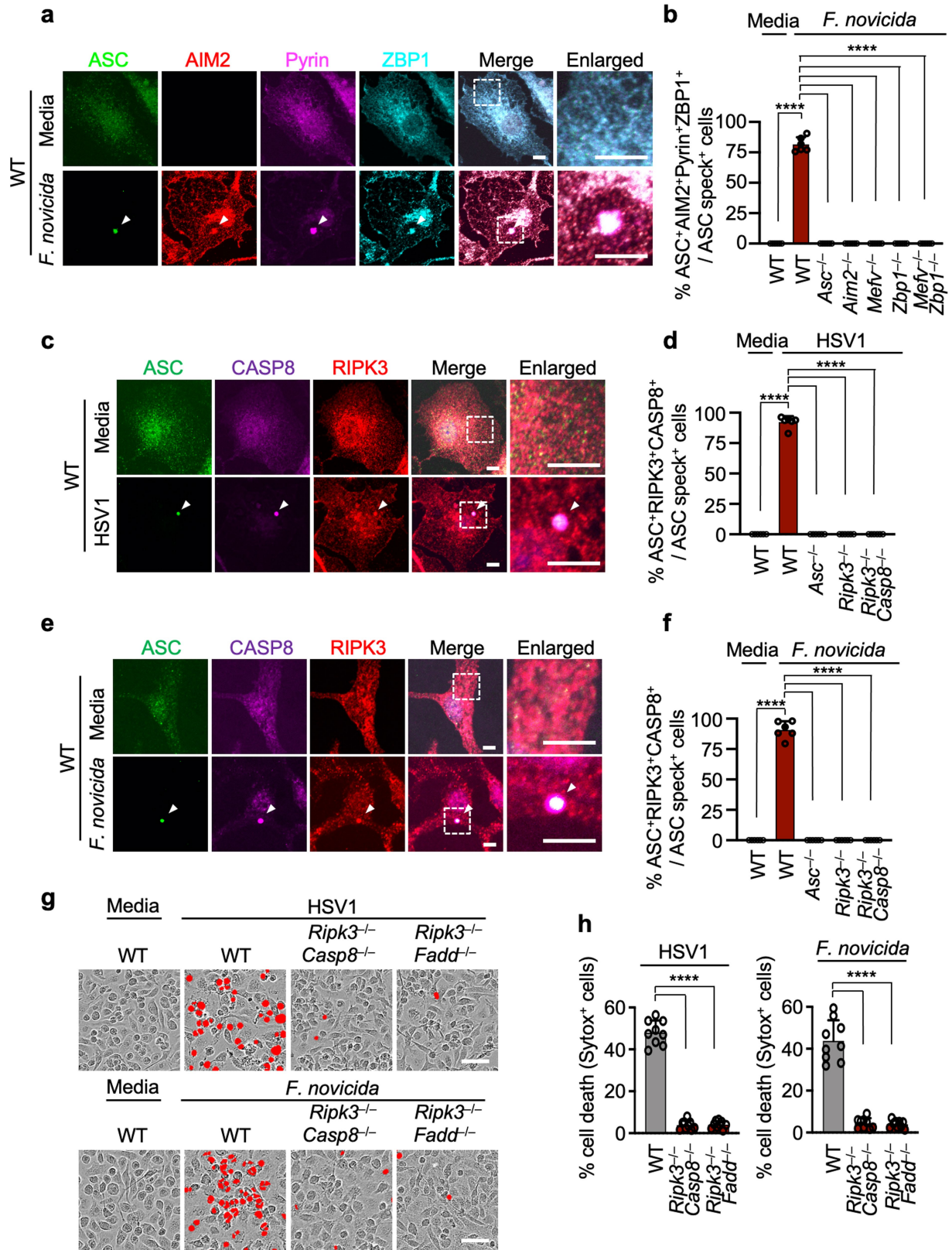
Extended Data Fig. 7 | The expression of Pyrin and ZBP1 is regulated by AIM2 during HSV1 and *F. novicida* infections. a–d, Relative expression of *Zbp1* (a, b) and *Mefv* (c, d) in wild type (WT), *Aim2*^{-/-}, *Asc*^{-/-} or *Casp1*^{-/-} bone marrow-derived macrophages (BMDMs) after HSV1 (a, c) or *F. novicida* (b, d) infections. Expression presented relative to that of the control gene *Gapdh*. Data are mean \pm s.e.m. from three independent experiments. *****P* < 0.0001 (one-way ANOVA with Dunnett’s multiple comparisons test, *n* = 6). e, f, Release

of IFN- β following HSV1 (e) or *F. novicida* (f) infections. Data are mean \pm s.e.m. *****P* < 0.0001 (one-way ANOVA with Dunnett’s multiple comparisons test; *n* = 6 from 3 biologically independent samples). Exact *P* values are presented in Supplementary Table 1. g, h, Immunoblot analysis of ZBP1 and Pyrin expression in the indicated BMDMs after HSV1 (g) or *F. novicida* (h) infections with or without IFN- β treatment. Data are representative of at least three independent experiments. For gel source data, see Supplementary Figure 1.



Extended Data Fig. 8 | Loss of AIM2 or combined loss of Pyrin and ZBP1 prevents the formation of the AIM2 complex during HSV1 and *F. novicida* infections. **a, b,** Immunoprecipitation (IP) in wild type (WT), *Aim2*^{-/-}, *Mefv*^{-/-}, *Zbp1*^{-/-} or *Mefv*^{-/-}*Zbp1*^{-/-} bone marrow-derived macrophages (BMDMs) with either IgG control antibodies or anti-ASC antibodies after HSV1 (a) or

F. novicida (b) infection. Data are representative of three independent experiments. **c, d,** IP in WT, *Ripk3*^{-/-}, *Ripk3*^{-/-}*Casp8*^{-/-} or *Ripk3*^{-/-}*Fadd*^{-/-} BMDMs with either IgG control antibodies or anti-ASC antibodies after HSV1 (c) or *F. novicida* (d) infection. Data are representative of three independent experiments. For gel source data, see Supplementary Figure 1.

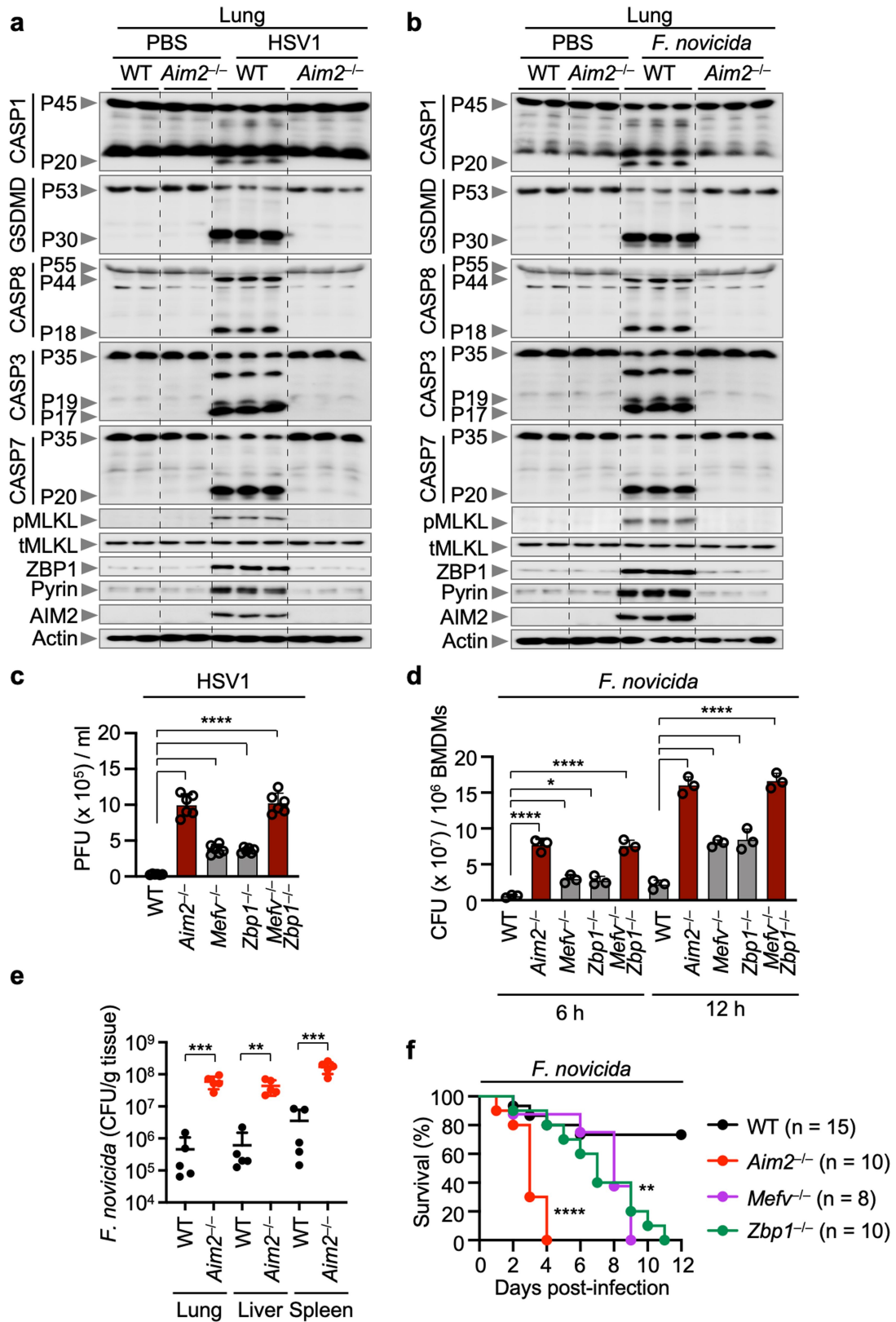


Extended Data Fig. 9 | See next page for caption.

Extended Data Fig. 9 | ASC speck colocalizes with AIM2, Pyrin and ZBP1, caspase-8 and RIPK3 in the same cell during HSV1 and *F. novicida* infections, and formation of this complex drives cell death.

a, Immunofluorescence images of wild type (WT) bone marrow-derived macrophages (BMDMs) at 12 h after *F. novicida* infection. Scale bars, 5 μ m. Arrowheads indicate the ASC speck. Images are representative of three independent experiments. **b**, Quantification of the percentage of cells with ASC⁺AIM2⁺Pyrin⁺ZBP1⁺ specks among the ASC speck⁺ cells. Data are mean \pm s.e.m. **** P < 0.0001 (one-way ANOVA with Dunnett's multiple comparisons test; n = 6 from 3 biologically independent samples). **c**, Immunofluorescence images of WT BMDMs at 12 h after HSV1 infection. Scale bars, 5 μ m. Arrowheads indicate the ASC speck. Images are representative of three independent experiments. **d**, Quantification of the percentage of cells with ASC⁺RIPK3⁺CASP8⁺ specks among the ASC speck⁺ cells.

Data are mean \pm s.e.m. **** P < 0.0001 (one-way ANOVA with Dunnett's multiple comparisons test; n = 6 from 3 biologically independent samples). **e**, Immunofluorescence images of WT BMDMs at 12 h after *F. novicida* infection. Scale bars, 5 μ m. Arrowheads indicate the ASC speck. Images are representative of three independent experiments. **f**, Quantification of the percentage of cells with ASC⁺RIPK3⁺CASP8⁺ specks among the ASC speck⁺ cells. Data are mean \pm s.e.m. **** P < 0.0001 (one-way ANOVA with Dunnett's multiple comparisons test; n = 6 from 3 biologically independent samples). **g**, Cell death in WT, *Ripk3*^{-/-}*Casp8*^{-/-} or *Ripk3*^{-/-}*Fadd*^{-/-} BMDMs at 16 h post-infection with HSV1 or *F. novicida*. Red indicates dead cells. Data are representative of at least three independent experiments. Scale bar, 50 μ m. **h**, Quantification of the cell death from (**g**). Data are mean \pm s.e.m. **** P < 0.0001 (one-way ANOVA with Dunnett's multiple comparisons test; n = 9 from 3 biologically independent samples). Exact P values are presented in Supplementary Table 1.



Extended Data Fig. 10 | See next page for caption.

Extended Data Fig. 10 | AIM2 regulates Pyrin and ZBP1 expression in vivo, and AIM2 provides host protection against HSV1 and *F. novicida*.

a, b, Immunoblot analysis of pro- (P45) and activated (P20) caspase-1 (CASP1), pro- (P53) and activated (P30) gasdermin D (GSDMD), pro- (P55) and cleaved (P18) caspase-8 (CASP8), pro- (P35) and cleaved (P17/P19) caspase-3 (CASP3), pro- (P35) and cleaved (P20) caspase-7 (CASP7), phosphorylated MLKL (pMLKL), total MLKL (tMLKL), ZBP1, Pyrin and AIM2 in lung from uninfected animals (PBS) or wild type (WT) or *Aim2*^{-/-} mice 3 days after HSV1 (**a**) or *F. novicida* (**b**) infection. Each lane indicates independent biological replicates. **c**, Viral quantification in WT, *Aim2*^{-/-}, *Mefv*^{-/-}, *Zbp1*^{-/-} or *Mefv*^{-/-}*Zbp1*^{-/-} BMDMs at 16 h post-infection with HSV1. Data are mean ± s.e.m. *****P* < 0.0001 (one-way ANOVA with Dunnett's multiple comparisons test; *n* = 6 from 3 biologically

independent samples). **d**, Bacterial quantification in WT, *Aim2*^{-/-}, *Mefv*^{-/-}, *Zbp1*^{-/-} or *Mefv*^{-/-}*Zbp1*^{-/-} BMDMs after *F. novicida* infection. Data are mean ± s.e.m. **P* < 0.05 and *****P* < 0.0001 (one-way ANOVA with Dunnett's multiple comparisons test; *n* = 3 from 3 biologically independent samples). **e**, In vivo bacterial quantification in lung, liver or spleen from WT or *Aim2*^{-/-} mice 2 days after *F. novicida* infection (*n* = 5). Each symbol represents one mouse. Data are pooled from two independent experiments. Data are mean ± s.e.m. ***P* < 0.01 and ****P* < 0.001 (two-tailed t-test). **f**, Survival of WT, *Aim2*^{-/-}, *Mefv*^{-/-} and *Zbp1*^{-/-} mice infected subcutaneously with 5 × 10⁵ CFU of *F. novicida* in 200 µl PBS. Survival data are pooled from three independent experiments. ***P* < 0.01; *****P* < 0.0001 (log-rank (Mantel-Cox) test). Exact *P* values are presented in Supplementary Table 1. For gel source data, see Supplementary Figure 1.

Reporting Summary

Nature Research wishes to improve the reproducibility of the work that we publish. This form provides structure for consistency and transparency in reporting. For further information on Nature Research policies, see [Authors & Referees](#) and the [Editorial Policy Checklist](#).

Statistics

For all statistical analyses, confirm that the following items are present in the figure legend, table legend, main text, or Methods section.

n/a Confirmed

- The exact sample size (n) for each experimental group/condition, given as a discrete number and unit of measurement
- A statement on whether measurements were taken from distinct samples or whether the same sample was measured repeatedly
- The statistical test(s) used AND whether they are one- or two-sided
Only common tests should be described solely by name; describe more complex techniques in the Methods section.
- A description of all covariates tested
- A description of any assumptions or corrections, such as tests of normality and adjustment for multiple comparisons
- A full description of the statistical parameters including central tendency (e.g. means) or other basic estimates (e.g. regression coefficient) AND variation (e.g. standard deviation) or associated estimates of uncertainty (e.g. confidence intervals)
- For null hypothesis testing, the test statistic (e.g. F , t , r) with confidence intervals, effect sizes, degrees of freedom and P value noted
Give P values as exact values whenever suitable.
- For Bayesian analysis, information on the choice of priors and Markov chain Monte Carlo settings
- For hierarchical and complex designs, identification of the appropriate level for tests and full reporting of outcomes
- Estimates of effect sizes (e.g. Cohen's d , Pearson's r), indicating how they were calculated

Our web collection on [statistics for biologists](#) contains articles on many of the points above.

Software and code

Policy information about [availability of computer code](#)

Data collection

Microscopy images were collected using manufacturer supplied software (IncuCyte S3). Confocal microscopy samples were visualized and imaged using a Zeiss LSM 780 NLO confocal microscope. For immunoblotting, membranes were developed with an Amersham imager.

Data analysis

For immunoblotting, images were analyzed with ImageJ (v1.53a). Graphpad Prism version 8 and IncuCyte S3 (v2018C) were used for data analysis.

For manuscripts utilizing custom algorithms or software that are central to the research but not yet described in published literature, software must be made available to editors/reviewers. We strongly encourage code deposition in a community repository (e.g. GitHub). See the Nature Research [guidelines for submitting code & software](#) for further information.

Data

Policy information about [availability of data](#)

All manuscripts must include a [data availability statement](#). This statement should provide the following information, where applicable:

- Accession codes, unique identifiers, or web links for publicly available datasets
- A list of figures that have associated raw data
- A description of any restrictions on data availability

The datasets generated and analyzed during the current study are contained within the manuscript and accompanying extended data figures and tables.

Field-specific reporting

Please select the one below that is the best fit for your research. If you are not sure, read the appropriate sections before making your selection.

- Life sciences Behavioural & social sciences Ecological, evolutionary & environmental sciences

For a reference copy of the document with all sections, see [nature.com/documents/nr-reporting-summary-flat.pdf](https://www.nature.com/documents/nr-reporting-summary-flat.pdf)

Life sciences study design

All studies must disclose on these points even when the disclosure is negative.

Sample size	Key experiments were repeated by independent researchers. If all 3 replicates gave similar results, experiments were considered as reproducible and completed. Prior sample size determination was not done. Based on our past studies, we concluded that the smallest number of animals per group should be seven. To arrive at this number, we used the JMP statistical package to perform a power analysis. Using parameters of alpha = 0.05; power = 80%; effect size = 50%; and standard deviation = 30% of the mean, we arrived at a group size of seven for a comparison between two groups. Groups of less than 7 were used in confirmatory analyses.
Data exclusions	ROUT test with Q-value of 0.1 as a cut-off was used to exclude outliers. The data exclusion criterion was pre-established. All data were retained if removing outliers could have resulted in a sample size of less than 3. No outliers were removed from the datasets reported.
Replication	Each experiment was performed with at least 3 biological replicates. All the reported results are from experiments in which every repeat gave similar results.
Randomization	For in vitro experiments, cells from the same pool of BMDMs were randomly split into separate wells and subjected to the treatments. For in vivo experiments, animals from the same cage were randomly selected for mock treatment or infection.
Blinding	Investigators were not blinded. None of the reported experiments require subjective decision making. Key experiments were repeated by independent researchers. Therefore, there was no need for blinding.

Reporting for specific materials, systems and methods

We require information from authors about some types of materials, experimental systems and methods used in many studies. Here, indicate whether each material, system or method listed is relevant to your study. If you are not sure if a list item applies to your research, read the appropriate section before selecting a response.

Materials & experimental systems		Methods	
n/a	Involved in the study	n/a	Involved in the study
<input type="checkbox"/>	<input checked="" type="checkbox"/> Antibodies	<input checked="" type="checkbox"/>	<input type="checkbox"/> ChIP-seq
<input type="checkbox"/>	<input checked="" type="checkbox"/> Eukaryotic cell lines	<input checked="" type="checkbox"/>	<input type="checkbox"/> Flow cytometry
<input checked="" type="checkbox"/>	<input type="checkbox"/> Palaeontology	<input checked="" type="checkbox"/>	<input type="checkbox"/> MRI-based neuroimaging
<input type="checkbox"/>	<input checked="" type="checkbox"/> Animals and other organisms		
<input checked="" type="checkbox"/>	<input type="checkbox"/> Human research participants		
<input checked="" type="checkbox"/>	<input type="checkbox"/> Clinical data		

Antibodies

Antibodies used	<p>Immunoblotting: anti-caspase-1 (AdipoGen, AG-20B-0042, 1:1000), anti-caspase-3 (CST, #9662, 1:1000), anti-cleaved caspase-3 (CST, #9661, 1:1000), anti-caspase-7 (CST, #9492, 1:1000), anti-cleaved caspase-7 (CST, #9491, 1:1000), anti-caspase-8 (CST, #4927, 1:1000), anti-cleaved caspase-8 (CST, #8592, 1:1000), anti-pRIPK3 (CST, #91702S, 1:1000), anti-RIPK3 (ProSci, #2283, 1:1000), anti-pMLKL (CST, #37333, 1:1000), anti-MLKL (Abgent, AP14272b, 1:1000), anti-GSDMD (Abcam, ab209845, 1:1000), anti-GSDME (Abcam, ab215191, 1:1000), anti-Pyrin (Abcam, ab195975, 1:1000), anti-AIM2 (Abcam, ab119791, 1:1000), anti-ZBP1 (AdipoGen, AG-20B-0010, 1:1000), anti-ASC (Millipore, #04-147, 1:1000), anti-RIPK1 (CST, 3493, 1:1000), anti-FADD (Millipore, 05-486, 1:1000), anti-β-actin (Proteintech, 66009-1-IG, 1:5000), human anti-caspase-1 (R&D systems; Cat# MAB6215), human anti-β-actin (CST, 4970, 1:1000); secondary anti-rabbit (111-035-047) or anti-mouse (315-035-047) HRP antibodies from Jackson ImmunoResearch Laboratories.</p> <p>Microscopy: Alexa Fluor 488 (ThermoFisher, A20181)-conjugated anti-ASC (Millipore, 04-147), Alexa Fluor 532 (ThermoFisher, A20182)-conjugated anti-AIM2 (Abcam, ab119791), Alexa Fluor 568 (ThermoFisher, A20184)-conjugated anti-Pyrin (Abcam, ab195975), Alexa Fluor 647 (ThermoFisher, A20186)-conjugated anti-ZBP1 (AdipoGen, AG-20B-0010), Alexa Fluor 568 (ThermoFisher, A20184)-conjugated anti-RIPK3 (ProSci, #2283), or Alexa Fluor 647 (ThermoFisher, A20186)-conjugated anti-caspase-8 (Enzo, 1G12) were made according to the manufacturer's instructions and used with 1:100 dilutions.</p>
Validation	All antibodies were validated by their source company. anti-caspase-1 (AdipoGen, AG-20B-0042): Measuring the inflammasome: O. Gross; Methods Mol. Biol. (2012). https://doi.org/10.1007/978-1-62703-321-9_10

adipogen.com/ag-20b-0042-anti-caspase-1-p20-mouse-mab-casper-1.html
 anti-caspase-3 (CST, #9662): Type I interferon signaling mediates Mycobacterium tuberculosis-induced macrophage death: L. Zhang; J. Exp. Med. (2021). <https://www.cellsignal.com/products/primary-antibodies/caspase-3-antibody/9662>
 anti-cleaved caspase-3 (CST, #9661): RIPK1 Distinctly Regulates Yersinia-Induced Inflammatory Cell Death, PANoptosis: R K Subbarao Malireddi; Immunohorizons (2020). <https://www.cellsignal.com/products/primary-antibodies/cleaved-caspase-3-asp175-antibody/9661>
 anti-caspase-7 (CST, #9492): RIPK1 Distinctly Regulates Yersinia-Induced Inflammatory Cell Death, PANoptosis: R K Subbarao Malireddi; Immunohorizons (2020). <https://www.cellsignal.com/products/primary-antibodies/caspase-7-antibody/9492>
 anti-cleaved caspase-7 (CST, #9491): RIPK1 Distinctly Regulates Yersinia-Induced Inflammatory Cell Death, PANoptosis: R K Subbarao Malireddi; Immunohorizons (2020). <https://www.cellsignal.com/products/primary-antibodies/cleaved-caspase-7-asp198-antibody/9491>
 anti-caspase-8 (CST, #4927): Caspase-6 Is a Key Regulator of Innate Immunity, Inflammasome Activation, and Host Defense: Min Zheng; Cell (2020). <https://www.cellsignal.com/products/primary-antibodies/caspase-8-antibody-mouse-specific/4927>
 anti-cleaved caspase-8 (CST, #8592): Caspase-6 Is a Key Regulator of Innate Immunity, Inflammasome Activation, and Host Defense: Min Zheng; Cell (2020). <https://www.cellsignal.com/products/primary-antibodies/caspase-8-antibody-mouse-specific/8592>
 anti-pRIPK3 (CST, #91702S): Diverse sequence determinants control human and mouse receptor interacting protein 3 (RIP3) and mixed lineage kinase domain-like (MLKL) interaction in necroptotic signaling: Wanze Chen; J. Biol. Chem. (2013). https://www.cellsignal.com/products/primary-antibodies/phospho-rip3-thr231-ser232-e7s1r-rabbit-mab/91702?site-search-type=Products&N=4294956287&Ntt=91702s&fromPage=plp&_requestid=4790034
 anti-RIPK3 (ProSci, #2283): Receptor interacting protein kinase-3 determines cellular necrotic response to TNF-alpha: Sudan He; Cell (2009). <https://www.prosci-inc.com/rip3-antibody-2283.html>
 anti-pMLKL (CST, #37333): Caspase-6 Is a Key Regulator of Innate Immunity, Inflammasome Activation, and Host Defense. Min Zheng; Cell (2020). <https://www.cellsignal.com/products/primary-antibodies/phospho-mlkl-ser345-d6e3g-rabbit-mab/37333>
 anti-MLKL (Abgent, AP14272b): Caspase-6 Is a Key Regulator of Innate Immunity, Inflammasome Activation, and Host Defense. Min Zheng; Cell (2020). <https://www.citeab.com/antibodies/240195-ap14272b-m-mlkl-antibody-c-term>
 anti-GSDMD (Abcam, ab209845): Caspase-6 Is a Key Regulator of Innate Immunity, Inflammasome Activation, and Host Defense: Min Zheng; Cell (2020). <https://www.abcam.com/gsdmd-antibody-epr19828-ab209845.html>
 anti-GSDME (Abcam, ab215191): Structural Mechanism for GSDMD Targeting by Autoprocessed Caspases in Pyroptosis: Kun Wang; Cell (2020). <https://www.abcam.com/dfna5gsdme-antibody-epr19859-n-terminal-ab215191.html>
 anti-Pyrrin (Abcam, ab195975): TNF/TNFR axis promotes pyrin inflammasome activation and distinctly modulates pyrin inflammasomopathy: Deepika Sharma; J. Clin. Invest. (2019). <https://www.abcam.com/pyrin-antibody-epr18676-ab195975.html>
 anti-AIM2 (Abcam, ab119791): A prodrug of epigallocatechin-3-gallate alleviates high glucose-induced pro-angiogenic factor production by inhibiting the ROS/TXNIP/NLRP3 inflammasome axis in retinal Müller cells: JingxiaDu; Experimental Eye Research (2020). <https://www.abcam.com/aim2-antibody-ab119791.html>
 anti-ZBP1 (AdipoGen, AG-20B-0010): Caspase-6 Is a Key Regulator of Innate Immunity, Inflammasome Activation, and Host Defense: Min Zheng; Cell (2020). <https://adipogen.com/ag-20b-0010-anti-zbp1-mab-zippy-1.html>
 anti-ASC (Millipore, #04-147): HMGB1 promotes the activation of NLRP3 and caspase-8 inflammasomes via NF-kB pathway in acute glaucoma: W. Chi; J Neuroinflammation (2015).. https://www.emdmillipore.com/US/en/product/Anti-ASC-Antibody-clone-2E1-7,MM_NF-04-147?ReferrerURL=https%3A%2F%2Fwww.google.com%2F&bd=1
 anti-ASC (AdipoGen, AG-25B-006-C100): Human NLRP1 is a sensor for double-stranded RNA. S. Bauernfried; Science (2021). <https://adipogen.com/ag-25b-0006-anti-asc-pab-al177.html/>
 anti-RIPK1 (CST, 3493): Caspase-6 Is a Key Regulator of Innate Immunity, Inflammasome Activation, and Host Defense: Min Zheng; Cell (2020). <https://www.cellsignal.com/products/primary-antibodies/rip-d94c12-xp-rabbit-mab/3493>
 anti-FADD (Millipore, 05-486): Identification of the PANoptosome: A Molecular Platform Triggering Pyroptosis, Apoptosis, and Necroptosis (PANoptosis): Shelbi Christgen; Frontiers in Cellular and Infection Microbiology (2020). https://www.emdmillipore.com/US/en/product/Anti-FADD-Antibody-clone-1F7,MM_NF-05-486
 anti-β-actin (Proteintech, 66009-1-IG): Caspase-6 Is a Key Regulator of Innate Immunity, Inflammasome Activation, and Host Defense: Min Zheng; Cell (2020). <https://www.ptglab.com/products/Pan-Actin-Antibody-66009-1-ig.htm>
 human anti-caspase-1 (R&D systems; Cat# MAB6215): Influenza restriction factor MxA functions as inflammasome sensor in the respiratory epithelium: Sangjoon Lee; Science Immunology (2019). https://www.rndsystems.com/products/human-caspase-1-antibody-661228_mab6215
 human anti-β-actin (CST, 4970): Activation of caspase-3 is an initial step triggering accelerated muscle proteolysis in catabolic conditions: Jie Du; The Journal of Clinical Investigation (2004). <https://www.cellsignal.com/products/primary-antibodies/b-actin-13e5-rabbit-mab/4970>

Eukaryotic cell lines

Policy information about [cell lines](#)

Cell line source(s)

THP-1: ATCC® TIB-202™

Authentication

The THP-1 cell line was purchased directly from ATCC and was not further authenticated in our lab.

Mycoplasma contamination

Cells were tested for mycoplasma contamination using mycoplasma detection PCR and were found to be negative for mycoplasma contamination.

Commonly misidentified lines
(See [ICLAC](#) register)

Commonly misidentified lines have not been used in this study.

Animals and other organisms

Policy information about [studies involving animals](#); [ARRIVE guidelines](#) recommended for reporting animal research

Laboratory animals

All mice were bred and maintained in a specific pathogen-free facility at the Animal Resources Center at St. Jude Children's Research Hospital and were backcrossed to the C57BL/6 background (J substrain) for at least 10 generations. Both male and female mice were used in this study; age- and sex-matched 6- to 8-week-old mice were used for in vivo and 6- to 12-week-old mice were used for in vitro studies. Cohoused animals were used for in vivo analyses. Mice were housed in 20-23.3 degrees Celsius and 30-70% humidity with 12 h light/dark cycles and were fed standard chow.

Wild animals

The study did not involve wild animals.

Field-collected samples

The study did not involve field collected samples.

Ethics oversight

All mice were bred at St. Jude. Animal studies were conducted in accordance with protocols approved by the St. Jude Animal Care and Use Committee.

Note that full information on the approval of the study protocol must also be provided in the manuscript.